The Isotope Effect on Proton Conduction and Glass Transition in Phosphoric Acid

A Thesis Presented for the
Master of Science
Degree
The University of Tennessee, Knoxville

Maximilian Ferdinand Heres
August 2014

Copyright © 2014 by Maximilian Ferdinand Heres
All rights reserved.

ACKNOWLEDGEMENTS

This work would not have been possible without extensive support and encouragement from my advisor Dr. Alexei P. Sokolov and the members of the research group. I especially want to thank Dr. Yangyang Wang for his mentorship, guidance and instruction throughout my research. I would like to express my gratitude to my committee members Dr. Robert Compton and Dr. Jaan Mannik.

I also thank Dr. Tomonori Saito, Dr. Dmitry Voylov, Philip Griffin and Adam Holt for many fruitful discussions and ideas. No words can express my gratitude to my family and friends who have stood by my side during the good times and tragedies of my life during graduate school; especial Mike Bowman, Matthew Bishop, and Leah Kraft. I would not have made it without their support.

ABSTRACT

Hydrogen fuel cells combine hydrogen and oxygen to create water and electricity. Polymer electrolyte membranes (PEM) make up barriers within the fuel cell allowing only protons to pass through, while keeping other components separate. Many PEM contain phosphoric acid (PA) as a building block due to its excellent proton conducting properties. Improved ionic conductivity in PEM can lead to the development of better, more efficient fuel cells.

While ionic conductivity in PA at high temperatures is extensively characterized, the low temperature dynamics are not so well explored. Below the glass transition, molecular motion is frozen and proton motion is forced to occur via local, intermolecular hopping. The Grotthuss mechanism of proton transport describes a relay-type proton motion, in which the jump of a proton to a neighboring molecule is followed by a succeeding proton jump of a different proton. Proton hopping is faster than molecular diffusion of a charged molecule, i.e. the Grotthuss mechanism allows for extraordinarily high proton conduction.

Isotopic substitution of hydrogen with deuterium alters the mass of the moving particle, while keeping electric charge unaffected. The isotope effect is defined as the ratio of reaction rates of different isotopes. Classically, the isotope effect on proton motion should be proportional to the ratio of the square root of mass. Experiments have shown that the isotope effect does not confine to the classical picture, but in reality is much larger. Isotopic exchange also affects glass transition. The temperature at which glass transition occurs is generally higher in materials containing the heavier isotope.

In the present work, effects of isotopic substitution on electrical and material characteristics of PA are investigated using broadband dielectric spectroscopy (BDS), differential scanning calorimetry (DSC) and Brillouin light scattering (BLS). Ionic conductivity was found to decrease in PA with the heavier isotope. Glass transition temperatures increased in the deuterated samples. In addition a strong change in ionic conductivity and glass transition temperature were observed between samples of different concentrations of acidity. Isotope effects do not follow the classical predictions, but exhibit much stronger changes.

TABLE OF CONTENTS

CHAPTER 1: INTRODUCTION 1
CHAPTER 2: LITERATURE OVERVIEW 3
The Glass Transition 3
Mechanism of Proton Diffusion 3
Conductivity Relaxation 6
Isotopes Effect 8
Theories of the Isotope Effect on Proton Motion 9
Isotope Effect on Glass Transition 12
The Model System Phosphoric Acid 13
Isotope Effect on the Glass Transition in Phosphoric Acid 14
Isotope effect on proton conduction in phosphoric acid 16
Research Objectives 18
CHAPTER 3: MATERIALS AND METHODS 19
Phosphoric Acid Nomenclature 19
Sample Preparation 21
Measurement Techniques 22
Broadband Dielectric Spectroscopy 22
Dielectric measurement 27
Differential Scanning Calorimetry 27
DSC Measurement 29
Brillouin Spectroscopy 30
Brillouin Measurement 34
CHAPTER 4: RESULTS AND DISCUSSION 35
Dielectric Data of Deuterated Phosphoric Acid 35
Glass Transition in Dielectric Spectroscopy 37
Differential Scanning Calorimetry 39
Brillouin Light Scattering 42
Glass Transition - Discussion 44
Proton Conduction and Conductivity Relaxation Time 46

DC. Conductivity 51
Discussion of Ionic Conductivity 55
CHAPTER 5: CONCLUDING REMARKS 59
LIST OF REFERENCES 61
VITA 65

LIST OF FIGURES

Figure 2.1 Transport of hydronium cation (orange) in water (blue) via structural diffusion. In this representation oxygen (red) and hydrogen (white) remain in the initial bond structure within the molecule. 4

Figure 2.2 Grotthuss Mechanism of proton motion in which a proton (white) breaks a hydrogen bond with the oxygen (red) and hops to a neighboring water molecule (blue). When the excess proton is bound to a water molecule it forms a hydronium (orange). Then another proton from the hydronium moves from location B to C. 6

Figure 2.3 Graph showing the transition from super Arrhenius to Arrhenius behavior of conductivity relaxation time above and below the glass transition, respectively. The red line indicates the glass transition temperature. 8

Figure 2.4 Double-well potential with classical a) and semi-classical b) descriptions. The ion has to overcome an energy barrier E in order to jump to the neighboring molecule. Semi-classical theory includes ground state energy defined by zero point vibrations which reduce the required energy to ED and EH for deuterium (D) and hydrogen (H), respectively..... 11

Figure 2.5 Neat Phosphoric Acid H3PO4. Symmetric structure and proton donor and acceptor sites allow for excellent proton conduction. 14

Figure 2.6 Walden plot of different concentrations of phosphoric acid. Concentration is represented in the molar ratio, R, of P_2O_5 (phosphoric acid without any water) to H_2O ranging from R=1.5 to R=5 [34]. 17

Figure 3.1 Representation of orthophosphoric H_3PO_4, pyrophosphoric $H_4P_2O_7$, triphosphoric $H_5P_3O_{10}$ and tetraphosphoric acid $H_6P_4O_{13}$..... 19

Figure 3.2 Schematic of Novocontrol alpha analyzer used to measure the impedance of the sample Zs. The potentials U1 and U2 as well as a resistance R are used to measure Zs [41]. 26

Figure 3.3 Heat flow into a material is depicted upon heating. Temperature range from glassy to molten state. Thermodynamic processes of a material, such as glass transition, crystallization and melting are depicted. 29

Figure 3.4 The interaction of incoming wave vector, ki, and refracted wavevector, kf, result in the scattered wave vector q. The scattering angle is indicated by θ [42]. 31

Figure 3.5 Schematic of elastic, quasi-elastic, and inelastic light scattering as a function on change of frequency [42]. 32

Figure 3.6 Raw Brillouin scattering data of a deuterated phosphoric acid sample with concentration R=5. Temperatures 170K, 210K, and 230K are shown in black, green and red, respectively. 34

Figure 4.1: Dielectric permittivity ε', imaginary dielectric modulus M", and the real part of electric conductivity σ' of P2O51: 1.5D2O are plotted versus frequency in the top, center

and bottom part respectively. The depicted temperatures range from -60℃ to -30℃ in increments of 5℃. 36

Figure 4.2 Conductivity relaxation time τσ of deuterated phosphoric acid at different concentrations, a), and the comparison to the hydrated counter parts, b), shown in Arrhenius plots. The shown molar ratios correspond to R=1.5 (magenta star), R=2.0 (orange triangle), R=2.5 (green hexagon), R=3.0 (blue diamond), R=4 (red circle) and R=5 (black square) for the deuterated (closed) and hydrated (open) symbols respectively. 38

Figure 4.3 The heat flow of different concentrations of deuterated phosphoric acids as measured on the heating cycle via Differential Scanning Calorimetry (Exo Up). Various concentrations are indicated on the plot. Tg appears as an endothermic process. The sample with the ratio R=3 corresponds to neat phosphoric acid (D3PO4) which crystalized at around 273K. 40

Figure 4.4 Glass transition temperatures of deuterated (red) and hydrogenated (blue) phosphoric acid are compared to data from literature Aihara et al. [22] (green) and Corti et al. [33] (black). Tg is plotted versus w2 which is the weight fraction of P2O5 of the sample for easy extrapolation from zero to one. The lines indicate the Gordon Taylor fit for each data set corresponding to the color. 42

Figure 4.5 Average Brillouin frequency of deuterated (closed) and hydrogenated (open) phosphoric acid at R=1.5 (blue) and R=5 (green) plotted against temperature. The inset shows the derivative of frequency with temperature across the glass transition. 43

Figure 4.6 Comparison of glass transition temperatures obtained using DSC (black squares), dielectric spectroscopy (red circles) and Brillouin light scattering (green triangles). Deuterated and hydrogenated samples are represented by closed and open symbols, respectively. The insert shows the difference in the glass transition temperatures ΔTg between deuterated and hydrogenated samples with half filled symbols of the same color scheme. 45

Figure 4.7Log_{10} of conductivity relaxation time τσ of deuterated phosphoric acid at different water concentrations vs inverse temperature normalized to their Tg. 47

Figure 4.8 Log_{10} of conductivity relaxation time at the glass transition of deuterated (blue square) and hydrogenated phosphoric acid (red square). The insert shows the ratio of the above τσ(D)/τσ(H) at their Tg's vs concentrationR. The expected value of √2 is indicated by a red dashed line. 49

Figure 4.9 Activation Energies of ion conductivity in deuterated (red) and hydrogenated (blue) Phosphoric acid extracted from the Arrhenius fit of τσ at T<Tg. A minimum in Ea is observed in both cases at R=2.5. The insert shows the ratio of the activation energies for deuterated and hydrogenated samples. 50

Figure 4.10 Log_{10} of DC conductivity στ of deuterated phosphoric acid at different concentrations a) and the comparison to the hydrated counter parts b) shown in Arrhenius plots. The shown molar ratios correspond to R=1.5 (magenta star), R=2.0 (orange triangle), R=2.5 (green hexagon), R=3.0 (blue diamond), R=4 (red circle) and R=5 (black square) for the deuterated (closed) and hydrogenated (open) samples, respectively. 52

Figure 4.11 Ratio of $\sigma\tau$ in hydrogenated phosphoric acid to $\sigma\tau$ in deuterated phosphoric acid vs. 1000/T. The red dotted line indicates a value of $\sqrt{2}$. The molar ratios correspond to R=1.5 (magenta star), R=2.0 (orange triangle), R=2.5 (green hexagon), R=3.0 (blue diamond), R=4 (red circle) and R=5 (black square)..... 53

Figure 4.12 shows $\sigma\tau$ of deuterated phosphoric acid at Ratios R=1.5, 2.5, 5.0 (indicated on plot). The VFT (red) and Cohen Grest (green) fitting functions are extrapolated to $\sigma(T = \infty)$. The insert shows the ratio of the $\sigma(T = \infty)$ in hydrogenated to $\sigma(T = \infty)$ in deuterated phosphoric acids obtained from the VFT fit (red squares) and Cohen Grest fit (black squares). The blue squares denote the same ratio taken from the experimental data at 50℃. 55

CHAPTER 1:

INTRODUCTION

A large part of the current trend towards a “green” future lies not only in the development of new ways of harvesting sustainable energy, but also in efficient and environmentally friendly ways of storing this energy where it is needed. In today’s automotive industry the prominent method of avoiding the uses of fossil fuels and its environmentally hazardous and wasteful conversion into kinetic energy, is the use of electric motors as a replacement of the internal combustion motor. Advantages of electric motors to those powered by petroleum include a more favorable power and torque curve, as well as greater efficiency. Vehicles propelled by electric power based on current technology are limited by volume, weight and cost of elaborate energy storage systems. In the case of hydrogen-powered vehicles, oxygen and hydrogen are brought together within a fuel cell, releasing energy, which then powers the electric motor propelling the vehicle. Within these cells so called Polymer Electrolyte Membranes (PEM) separate different chambers of the fuel cell, allowing only hydrogen ion transfer. In practical applications the membranes need to exhibit high proton conductivity (on the order of milli-Siemens per centimeter) and withstand great amounts of physical and thermal stress.

The details of proton conduction mechanisms are a well-studied, yet controversial topic within the community. Phosphoric acid is known to be one of the best and most versatile proton conducting materials, making it a prime system for the study of proton transport mechanisms for energy applications. One way of studying the transfer of ion conducting substances is varying the mass of the conducting isotope. This variance influences both dynamic and electrical properties by changing conductive as well as glass transition behaviors. The goal of this report is to

understand the details of the conductivity mechanism by employing isotopic substitution. This thesis is presented in the following structure.

Chapter two reviews the current state of knowledge of how substitution of isotopes influences proton conduction and glass transition behavior, as well as the underlying theories related to each phenomenon. Phosphoric acid is a well-studied glass forming model-system for proton conduction and will be the main basis of this study.

Chapter three describes procedure of sample preparation and measurement used. The theory as well as the experimental techniques of broadband dielectric spectroscopy, differential scanning calorimetry and Brillouin light scattering are described.

Chapter four provides a detailed investigation of glass transition and proton conduction in deuterated phosphoric acid. These data are then compared to that of regular hydrogenated phosphoric acids, and the differences in conductivity, conductivity relaxation time and activation energy are presented.

Chapter five concludes this work by demonstrating that isotopic substitution in phosphoric acid causes an increase in the glass transition temperature, as demonstrated by all measurement techniques. The rate of proton conduction is lowered due to the increase of mass of the conducting ion, and the behavior cannot be explained by simple classic behavior.

CHAPTER 2:

LITERATURE OVERVIEW

The Glass Transition

Liquids that have the ability to be cooled from a liquid to a solid state without crystallizing are called vitreous liquids. The temperature at which a transition from liquid to solid state occurs without crystallization is referred to as the glass transition temperature, T_g. Above this temperature molecules rotate and diffuse. Below T_g, diffusion of individual molecules is frozen. The sample is trapped in a glassy, solid state. Glasses differ from crystalline solids due to the lack of long-range molecular order. The change of molecular dynamics upon vitrification affects the material properties. The temperature dependence of viscosity, conductivity and elastic constants exhibit a measurable change when the material is cooled below T_g [1-3].

The behavior of proton conductivity across a wide temperature range, including the glass transition, is of great importance to the development of proton conducting membranes for hydrogen fuel cells and other industrial applications. The impact of molecular dynamics on proton transport is discussed in the following section.

Mechanism of Proton Diffusion

In order to develop better proton conductors, it is crucial to first understand the mechanisms of proton motion. When the sample is in a liquid state, a particular proton can travel alongside the molecule to which it is bound. The molecule acts as a vehicle to transport the proton, and both the molecule and the proton diffuse through the system together. This method of proton transport is referred to as vehicle mechanism [4-6]. Water is used as an example to

demonstrate the main methods of proton diffusion due to its high proton conductivity as well as its simple molecular structure. Figure 2.1 depicts a scenario of proton transfer in water where an excess proton is bound to a specific water molecule, forming a hydronium, or H_3O^+ molecule [7, 8]. In Figure 2.1, the hydronium molecule is depicted in orange, while surrounding water molecules are represented by blue circles. The excess proton uses the water molecule as a vehicle to move through the system. In pure vehicle diffusion the excess proton can only move as fast as the hydronium molecule, making molecular diffusion of the hydronium ion through water rate determining.

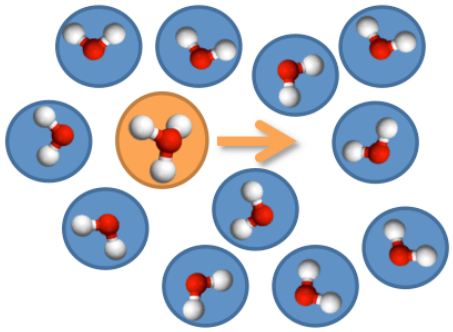

Figure 2.1 Transport of hydronium cation (orange) in water (blue) via structural diffusion. In this representation oxygen (red) and hydrogen (white) remain in the initial bond structure within the molecule.

Proton motion via the vehicle mechanism is strongly influenced by environmental factors such as temperature, density and pressure of the system. Viscosity increases with decreasing temperature, making it more difficult for protons to move. Diffusion is reduced at low temperatures until molecules become stationary. This occurs in glass forming systems below the

glass transition temperature. The mechanism of proton conductivity changes when molecular motion is restrained, and protons are limited to local hopping motion.

Another mechanism of proton diffusion is the Grotthuss mechanism [9-12]. This theory describes proton conduction via a proton hopping along a hydrogen-bonding network. Hydrogen bond cleavage and formation permits local proton jumping between neighboring molecules. This process does not require assistance of molecular diffusion, and can therefore occur at a much faster rate. It is commonly accepted that the Grotthuss mechanism is responsible for the abnormally high proton mobility in water [12]. An example of the Grotthuss mechanism of proton motion in water is depicted in Figure 2.2. The figure shows an excess proton, which is initially bound to a water molecule in location A. In order to jump, the proton has to first cleave its bond with the hydronium cation in order to form a new bond with the neighboring water molecule at location B. Proton motion continues when a different proton travels from location B to C in a similar fashion. This process does not require a specific proton to move throughout a system but rather assumes that once a proton has bonded to it's destine molecule, another proton continues the journey in the original proton's place. The proton that arrives at C is a different one than initially departed from location A. Hence proton transfer via Grotthuss mechanism is much faster than molecular diffusion and can therefore explain the abnormally high proton conduction in water [13].

Whether a proton moves via the vehicle or the Grotthuss mechanism depends on temperature and viscosity of the material. The distinction between methods of proton motion is important when considering the effects of conductivity relaxation and the isotope effects described in the following sections.

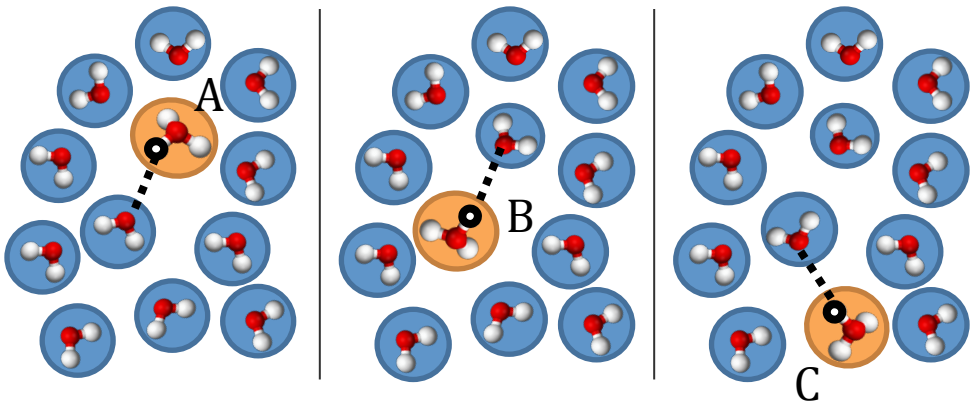

Figure 2.2 Grotthuss Mechanism of proton motion in which a proton (white) breaks a hydrogen bond with the oxygen (red) and hops to a neighboring water molecule (blue). When the excess proton is bound to a water molecule it forms a hydronium (orange). Then another proton from the hydronium moves from location B to C.

Conductivity Relaxation

Structural relaxation is a thermally activated process below T_g, which follows the Arrhenius equation [14]. This process occurs in the glassy regime, when the proton has to overcome a potential energy barrier in order to complete bond breaking and formation with the next molecule. A system, which is disturbed from equilibrium by an external force, seeks to return to the initial state. This is referred to as relaxation process. When the polarization of a dielectric material is disturbed by an external electric field, the corresponding equilibrium seeking process is referred to as conductivity relaxation. Equation eq. 2.1 displays the dependencies of the different factors influencing conductivity relaxation. In the Arrhenius equation, conductivity relaxation time, τ_σ, is expressed by the energy barrier that controls the proton to jump and is called the activation energy E_a.

$$\tau_\sigma = \tau_0 e^{\left(\frac{-E_a}{k_B T}\right)} \qquad eq.\ 2.1$$

τ_0 is a pre-factor that resembles the characteristic attempt time of a single ion jump. k_B represents the Boltzmann constant and T is the absolute temperature. E_a can be extracted from the Arrhenius fit when the logarithm of τ_σ is plotted versus inverse temperature, also called an Arrhenius plot. Below T_g $\mathrm{Log}_{10}(\tau_\sigma)$ displays a linear dependence on inverse temperature, justifying the applicability of the Arrhenius Law.

Above T_g, when the sample is in a liquid state, structural and conductivity relaxation exhibit super-Arrhenius behavior, meaning that dynamics show stronger temperature dependence than predicted by the Arrhenius equation. This is due to the fact that proton motion is aided by molecular motions in the liquid state [7]. Crossover of Arrhenius to super-Arrhenius temperature dependences at the glass transition has been observed in many other glass forming ionic conductors [14]. The phenomenological Vogel-Fulcher-Tammann (VFT) equation can be used to describe the conductivity relaxation time in the liquid state [15].

$$\tau_\sigma = \tau_0 e^{\left(\frac{B}{T-T_0}\right)} \qquad eq.\ 2.2$$

τ_0 is again the characteristic attempt time, though it is not necessarily the same value as τ_0 from the Arrhenius equation. T_0 is often described as an ideal glass transition temperature, and B is a material specific parameter.

The Cohen-Grest (CG) equation 2.3, below, is an alternative fitting function for relaxation processes in the glassy state [16]. It is similar to VFT, but introduces a variable C in the exponential. This parameter incorporates free volume and has been found to provide a more accurate fit [17].

$$\tau_\sigma = \tau_0 e^{\left(\frac{B}{T-T_0+\sqrt{(T-T_0)^2+CT}}\right)} \qquad eq.\ 2.3$$

Figure 2.3 is a sketch of conductivity relaxation time as a function of inverse temperature normalized to T_g. The red line indicates the glass transition temperature. A clear transition from Arrhenius to super Arrhenius temperature dependence is displayed at the glass transition. This figure demonstrates that the temperature dependence of τ_σ is getting steeper while the sample is cooled, and becomes linear while the sample is arrested in its glassy state.

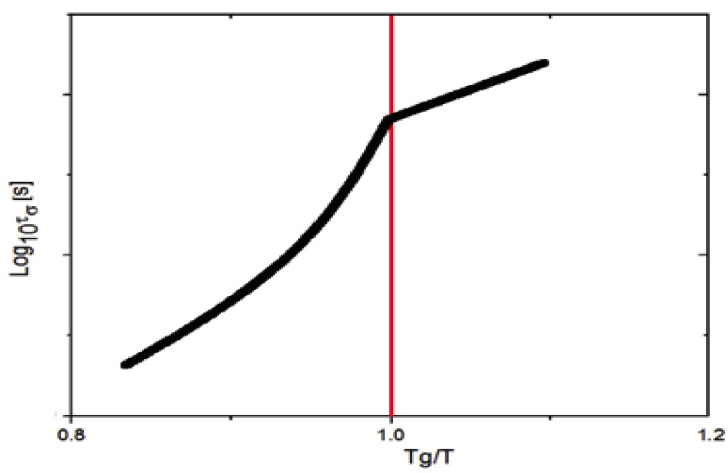

Figure 2.3 Graph showing the transition from super Arrhenius to Arrhenius behavior of conductivity relaxation time above and below the glass transition, respectively. The red line indicates the glass transition temperature.

Isotopes Effect

Now that we have discussed the dynamics as a function of temperature, it is interesting to determine how a change in mass of the ion affects proton conduction and glass transition. This is done using isotope exchange of the hydrogen atom. Isotopic substitution allows for a change in

mass of a chemical element, while retaining the electric charge. The additional mass can cause a variation in many material properties such as the glass transition temperature and ionic conductivity. The term isotope effect refers, in particular, to the ratio of transition rates of different isotopes. Hydrogen is the lightest element on the periodic table, consisting of only a proton and an electron. Deuterium is a heavier isotope consisting of an additional neutron bound to the proton in the nucleus. The mass of the electron is small in comparison to that of the proton and neutron, causing the additional neutron to increases the mass of the atom to nearly twofold. The third naturally occurring isotope of hydrogen, tritium, contains two additional neutrons over hydrogen. Although tritium has been studied in relation to proton conduction, the radioisotope is not a favorable material of study due to its unstable state [18]. The focus of this research lies in the comparison of the first two isotopes hydrogen and deuterium.

Since the net charge of the molecule is unaffected by the addition of a neutron, the variations in material properties are exclusively caused by the change in mass. The importance of comparing the isotope effect in hydrogen and deuterium as opposed to isotopes of different molecules lies in the severity of the mass change. Due to the light nature of the hydrogen, isotopic substitution with the heavier isotope deuterium presents the greatest relative mass increase of any atom. This is significant because it maximizes the effect that H/D exchange has on the sample. Before we examine the experimental data, it is important to study the theoretical implications of isotope exchange, presented in the following section.

Theories of the Isotope Effect on Proton Motion

The potential energy landscape of a single one-dimensional proton jump can be modeled as a double-well harmonic potential as shown in Figure 2.4. The minima of the potential

represent locations of initial and final molecular bonding sights. An activation energy of magnitude greater than or equal to the height of the potential barrier is required to induce a proton jump. The attempt frequency for a proton jump, ν_0, is described by the harmonic oscillator equation.

$$\nu_0 = \frac{1}{2\pi}\sqrt{\frac{k}{m}} \qquad \textit{eq. 2.4}$$

In this equation m is the mass of the particle in the well. The force constant k depends on the potential energy landscape, which is identical for the two isotopes [18-22]. The isotope effect on the conductivity relaxation time, τ_σ, should then be proportional to $\sqrt{2}$ through the relation $\tau = (2\pi\nu)^{-1}$.

$$\frac{\tau_D}{\tau_H} = \sqrt{\frac{m_D}{m_H}} = \sqrt{2} \qquad \textit{eq. 2.5}$$

However, experiments done by various researchers [21] show that the isotope effect in proton conduction is much stronger than $\sqrt{2}$. Since the purely classical theory disagrees with experimental data, the influences of quantum effects can be considered in order to improve the accuracy of the theory. The semi-classical theory incorporates the quantum mechanical concept of zero point vibrations into classical theory. According to a quantum mechanical view, a particle's lowest possible energy is the ground state energy E_0 described by Equation 2.6.

$$E_0 = \frac{1}{2}\hbar\nu \qquad \textit{eq. 2.6}$$

In this equation $\hbar$ is Planck's constant divided by 2π and ν is the frequency of hydrogen or deuterium oscillations. Deuterium has higher mass than hydrogen and following the above equation has a slower vibrational frequency ($\nu_D < \nu_H$). This indicates that hydrogen, which has

less mass than deuterium, has higher ground state energy than deuterium as depicted in Figure 2.4 b.

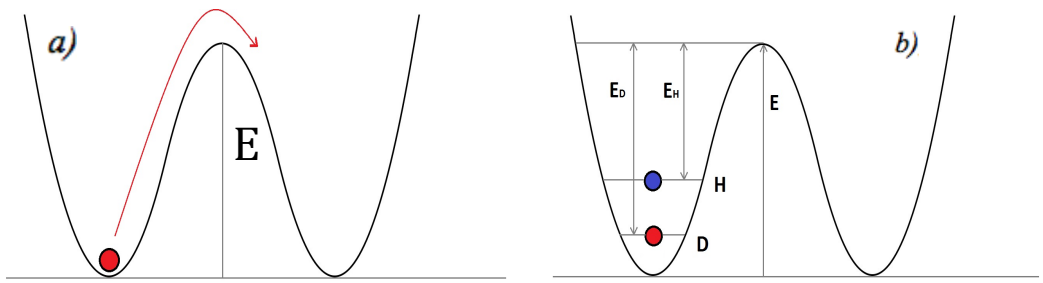

Figure 2.4 Double-well potential with classical a) and semi-classical b) descriptions. The ion has to overcome an energy barrier E in order to jump to the neighboring molecule. Semi-classical theory includes ground state energy defined by zero point vibrations which reduce the required energy to ED and EH for deuterium (D) and hydrogen (H), respectively.

The ground state energy assists the jumping particle by reducing the relative height of the energy barrier. Hydrogen has higher ground state energy compared to deuterium, therefore requiring less activation energy. The differences in E_a between isotopes further increase the isotope effect in proton conduction following the semi-classical theory.

Further expansions of the theory of proton conduction have been made in the attempt of predicting large isotope effect values. Another theory based on quantum mechanics considers tunneling effects as described by Nowick et al. [21]. Here the probability wave function has exponential dependence on the proton's mass, causing even slight mass modifications to result in an extraordinarily large isotope effects. However there is insufficient conclusive evidence to

support tunneling affects in proton conducting systems, and so this topic will not be discussed any further.

Isotope Effect on Glass Transition

Now that we have examined how the increased mass of the moving ion affects transport characteristics below the glass transition, we can look at the effects on the glass transition itself. The glass transition temperature is related to material properties such as density and viscosity. Isotopic substitution alters these material specific properties, therefore altering the glass transition temperature. In order to examine the isotope effect on the glass transition, it is favorable to study a material whose composition is greatly altered by deuteration. The comparison of water, H_2O, at $18\frac{g}{mol}$ with deuterated water, D_2O, at $20\frac{g}{mol}$ therefore provides significant change in molecular mass. Although oxygen is much heavier than hydrogen or deuterium, the deuteration of water still causes over 10% increase in mass of the molecule. D_2O is commonly referred to as heavy water. Determining the glass transition of water and heavy water presents a challenging task due to the formation of ice below 273K. Different methods such as hyper-quenching, confinement, and addition of impurities to the sample have been developed in order to suppress crystallization in water.

Many researchers have measured the glass transition of super-cooled water [23-25]. It is generally accepted that the T_g of water lays around 136K. The glass transition in deuterated water generally occurs around 140K, showing a change in the glass transition temperature, ΔT_g, at the glass transition of ~3-5K depending on the experiment and the phase of the super-cooled water. Recent dielectric relaxation spectroscopy measurements of low density and vapor

deposited amorphous water were performed in our group. Results showed that H/D substitution can alter the glass transition as much as $10 \pm 2K$ [26]. Small inconsistencies in sample preparation and variances in measurement techniques greatly impact the results of T_g measurements. Differences in phase states of water at low temperatures can also lead to inconsistent results. Disagreements about the glass transition of hyper-quenched water are therefore still ongoing.

An alternative to hyper-quenching the sample in order to avoid crystallization is the addition of a solute, such as a salt or an acid. These additives lower the freezing point of the solution. A study done by Kano at al. [27] focuses on the glass transition temperature of LiCl and $ZnCl_2$ solutions with both hydrogenated and deuterated water as studied via differential thermal analysis. T_g of the solutions exhibits concentration as well as isotopic dependence. Glass transition temperatures decrease with dilution and converge to the value of pure components in the dilute region. The samples prepared with D_2O exhibit higher glass transition temperatures than the ones prepared with H_2O. ΔT_g increases with dilution to above 4K for the LiCl samples and up to 1.7K for the $ZnCl_2$ sample within the measured range. The values for ΔT_g concur with those found in hyper-quenched sample. Other salts and acids can also be used in order to produce non-crystallizing water solutions [28, 29]. Phosphoric acid is a prime candidate for this research due to its superb glass transition properties as well as its proton conductivity.

The Model System Phosphoric Acid

Phosphoric acid is a weak acid and has the structure H_3PO_4 in its neat form as presented in Figure 2.5. Phosphoric acid has broad applications such as membrane materials in PEMs of modern hydrogen fuel cells [30, 31]. Phosphoric acid has the ability to form compound structures

at high concentrations up to P_2O_5, containing no water molecules at all. The advantage of phosphoric acid lies in dependence of its T_g on concentration. By varying the concentration of the acid, the T_g can be altered by almost 80K within an easily measurable window. Phosphoric acid is therefore ideal for measuring the concentration dependence of T_g.

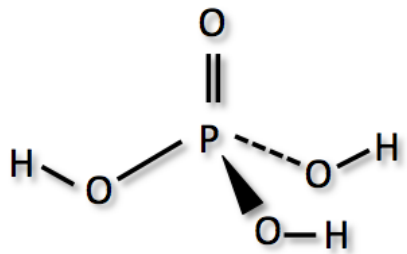

Figure 2.5 Neat Phosphoric Acid H_3PO_4. Symmetric structure and proton donor and acceptor sites allow for excellent proton conduction.

Isotope Effect on the Glass Transition in Phosphoric Acid

The glass transition of phosphoric acids has been studied using many different techniques including broad line nuclear magnetic resonance (NMR) [22, 32] differential scanning calorimetry (DSC) [33], and broadband dielectric spectroscopy (BDS) [34]. The concentrational dependence of the glass transition temperature in phosphoric acids shows expected temperature dependence by approaching T_g of the pure components. Highly concentrated phosphoric acid of the form P_2O_5 (T_g>590K) [35] is phosphoric acid without any water molecules. Dilution of phosphoric acid with water causes T_g to converge to that of pure water. Aihara et al. [22] uses an

exponential equation, eq. 2.7, to fit the data of the hydrated phosphoric acid samples to extrapolate the Glass transition temperature of pure water.

$$T_g = T_g^0 + \alpha e^{(\beta c)} \qquad eq.\ 2.7$$

Here T_g^0 is the glass transition temperature of pure water, c is the concentration of phosphoric acid and α and β are fitting parameters. In his paper Aihara et al. estimates T_g of pure water to be around 159.7K, which is much higher than commonly accepted. Research done by Corti et al. [33] dismisses Aihara's analysis due to lack of physical meaning of the phenomenological fitting equation. Instead Corti et al. propose the use of the Gordon Tailor equation (GT) [36] to fit the concentration dependence of T_g.

$$T_g = \frac{w_2 T_{g2} + w_1 k_{GT} T_{g1}}{w_2 + w_1 k_{GT}} \qquad eq.\ 2.8$$

The Gordon Tailor equation, eq. 2.8, which is based on free volume theory of liquids[37], uses the parameter k_{GT}, to define the ratio of the products of T_g, and the density at T_g of the individual ingredient. w_1, w_2 and T_{g1}, T_{g2} represent weight fraction and glass transition temperature of H_2O and P_2O_5 respectively. In his paper Corti et al. is able to fit DSC data using the Gordon Taylor equation, in the concentration range from w_2=0.839 to 0.361, which corresponds to the molar ratio R=1.51 to 13.94 of P_2O_5 to H_2O. Weight percentages are used instead of molar concentration in order to simplify the extrapolation to pure water (w_2). Though helpful in extrapolation of T_g, a representation with respect to weight percentage does not allow direct comparison between isotopes due to their mass difference. Corti et al. found the GT to provide a good fit for glass transition data in Phosphoric acid. In the concentrated region at R=1.51, the T_g=233K, while in the dilute region at R=13.9, T_g decreases by 80K to 153K. Neat phosphoric acid displays a T_g at around 190K. T_g data obtained from NMR by Aihara et al. [22] and DSC by

Corti et al. [33] follow the same trend when compared with acid concentration. Wang et al. [34] recently characterized hydrated phosphoric acid at various molar concentrations using BDS and rheological measurements in the low temperature regime. T_g values are in agreement with those provided in the literature, revealing Tg of the sample R=1.5 to be around 230K and of the sample R=5 to be around 170K. BDS determines T_g by measuring the characteristic relaxation time τ of structural relaxation, and is defined as the temperature at which τ=100 s. Comparing DC conductivity and conductivity relaxation time of hydrogenated and deuterated phosphoric acids at different concentrations can provide information on how the isotope affect alters proton motion.

Isotope effect on proton conduction in phosphoric acid

It is well known that dielectric properties show a distinctive thermal dependence. High temperature conductive properties, as well as glass transition behavior of phosphoric acid are extensively studied. Low temperature conductivity measurements above and below the glass transition have however been neglected in the current literature. Wang at al.[34] found that both DC conductivity σ_τ and conductivity relaxation time τ_σ exhibit a distinctive Arrhenius to super-Arrhenius crossover at the glass transition. The activation energy of ionic conductivity below T_g derived from the fit of the Arrhenius equation is on the order of 50-60 $\frac{kJ}{mol}$. Typical activation energies of proton conducting materials such as perovskite structured metal oxides [21] and protic ionic liquids [6, 20, 38, 39] range from 50-100 $\frac{kJ}{mol}$. Lower activation energy means that it is easier for a proton to conduct in a material. Therefore it can be concluded that phosphoric acid is a relatively good proton conducting material.

In a classical view, conductivity should be proportional to the fluidity of the material, since the diffusion of ions is severely inhibited in a viscous media. Walden first brought this relationship into perspective [40]. The so-called Walden plot compares molar conductivity to viscosity on a log-log plot. Figure 2.6 shows the Walden plot for different concentrations of hydrogenated phosphoric acid [34]. In the high temperature region, viscosity is low and has little friction effect on ionic conduction. Hence, phosphoric acid falls on the reference line of slope m=1 in the high temperature regime, indicating linear relationship between mobility and viscosity. At lower temperatures, however, high viscosity strongly limits molecular motion.

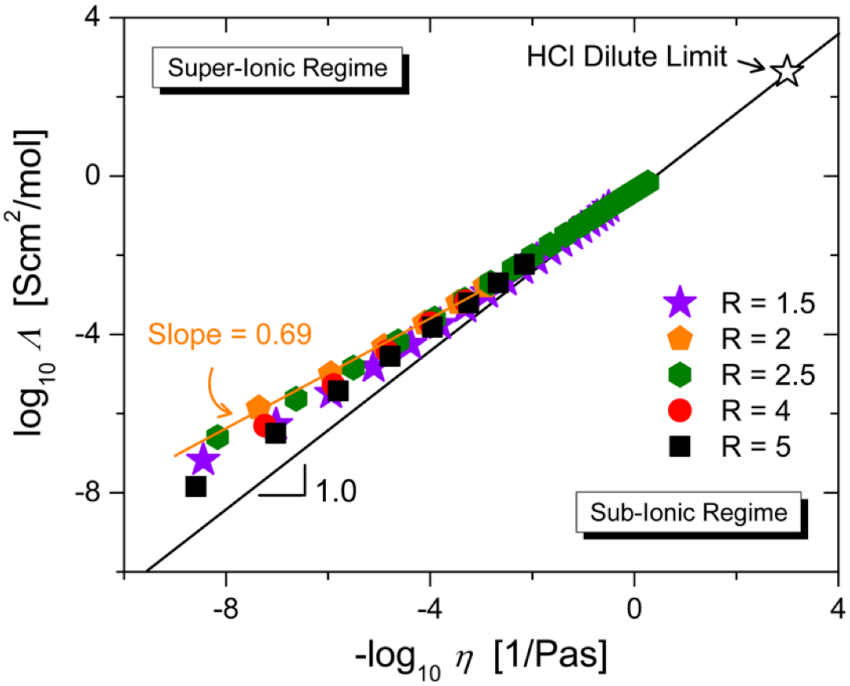

Figure 2.6 Walden plot of different concentrations of phosphoric acid. Concentration is represented in the molar ratio, R, of P_2O_5 (phosphoric acid without any water) to H_2O ranging from R=1.5 to R=5 [34].

A decoupling of proton motion from structural relaxation causes a divergence of the molar conductivity from linear relation with viscosity into the super ionic region. The slope of the data in the high viscosity region lies between 0.69 and 0.87 for varying R ratios. Physically this means that ions conduct faster than allowed by a direct correlation of mobility and viscosity. It would be interesting to examine the effects of isotopic exchange on proton/ionic conductivity.

Research Objectives

Phosphoric acid is an extensively studied proton conductor with a wide range of potential applications. Excellent glass forming and proton conducting properties make it an ideal material for proton conducting membranes in hydrogen fuel cell applications. Phosphoric acid also provides a suitable medium to study mechanisms of proton conductivity at low temperatures, a subject that has not yet been extensively explored. The goal of this research is to study the influence of the isotope effect on the glass transition and ionic conductivity of phosphoric acid.

We aim to determine how the isotope effect impacts the glass transition temperature in phosphoric acid at varying concentration. This can be achieved by measuring the difference in the glass transition temperature for H_3PO_4 in pure water and deuterated water. Isotopic exchange also alters ionic conductivity. By increasing the mass of the conducting ion by a factor of two, while keeping overall charge constant we can investigate the impact of mass on proton motion. In order to do so, we will compare DC conductivity and conductivity relaxation time of regular and deuterated phosphoric acid at different concentrations. Furthermore we hope that these studies will help to better understand the influence of quantum effects on proton motion.

CHAPTER 3:

MATERIALS AND METHODS

Phosphoric Acid Nomenclature

Neat Phosphoric acid, H_3PO_4 is also referred to as ortho-phosphoric acid. Phosphoric acid can form compounds of poly-phosphoric acid at different concentrations. These include the dimer $H_4P_2O_7$ (pyro-phosphoric acid) and the trimmer $H_5P_3O_{10}$ (tri-phosphoric acid). Pyro- and tri-phosphoric acids are the main building blocks of adenosine di-phosphate (ADP) and adenosine tri-phosphate (ATP) respectively, which are compounds responsible for energy transfer within biological systems. In its most concentrated form phosphoric acid forms phosphoric anhydride P_4O_{10} also denoted as P_2O_5 (phosphorus pentoxide). The consideration of different compounds is important because physical properties of the acid are highly dependent on the structure of the acid. P_2O_5 is usually crystalline with an estimated T_g of 590K [33]. The T_g of neat phosphoric acid on the other hand is lowered to roughly 190K. Further dilution to 85% H_3PO_4 aqueous solution, which is liquid at room temperature, lowers the T_g to ~177K [33]. The viscosity of phosphoric acid also severely decreases with dilution of aqueous phosphoric acid solutions. The concentration of phosphoric acid can be denoted in terms of weight

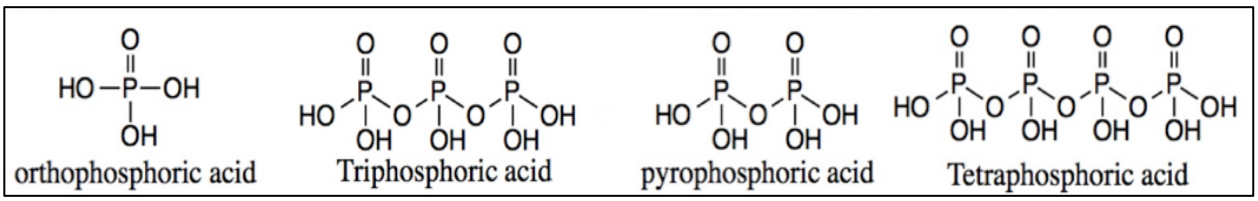

Figure 3.1 Representation of orthophosphoric H_3PO_4, pyrophosphoric $H_4P_2O_7$, triphosphoric $H_5P_3O_{10}$ and tetraphosphoric acid $H_6P_4O_{13}$

percentage (wt%) as well as molar ratio R, as shown in Table 3.1.Weight percentage is commonly denoted in terms of H_3PO_4 or P_2O_5. Representation in terms of weight percentage of H_3PO_4 can be misleading since acids, which are more concentrated than neat phosphoric acid, are represented in percentages that exceed 100%. Representation in the form of H_3PO_4+H_2O can also be misleading in acids with higher concentration than neat phosphoric acid. In these cases water has to be removed from neat phosphoric acid, denoted in a negative number of H_2O to denote the concentration. Expressing concentration in terms of weight percent of any standard is impractical in this case due to the mass differences of isotopes used in this study. Acid concentrations will be expressed in terms of molar ratio R of P_2O_5 to H_2O or D_2O.

$$P_2O_5\ (1{:}\,\mathrm{R})\ H_2O \qquad \text{and} \qquad P_2O_5\ (1{:}\,\mathrm{R})\ D_2O \qquad \textit{eq. 3.1}$$

This representation emphasizes a direct comparison of the number of molecules of each isotope rather than mass. Phosphorus pentoxide is a poly-phosphoric acid containing no hydrogen or deuterium atoms prior to sample preparation, and is therefore used as a standard representation in this study. A conversion chart of methods of determining concentrations is provided in *Table 3.1*.

Table 3.1 Conversion table of common methods of denoting concentrations of phosphoric acid.

R	$H_3PO_4 + H_2O$	wt% P_2O_5	wt% H_3PO_4
1.5	H_3PO_4 (-0.75) H_2O	84	116
2.0	H_3PO_4 (-0.5) H_2O	79.8	110
2.5	H_3PO_4 (-0.25) H_2O	75.9	105
3.0	H_3PO_4	72.4	100
4.0	H_3PO_4 + (0.5) H_2O	66.3	91.6
5.0	H_3PO_4 + 1H_2O	61.3	84.5
7.0	H_3PO_4 + 2H_2O	53.1	73.1
9.0	H_3PO_4 + 3H_2O	46.7	64.9
14.0	H_3PO_4 + 11H_2O	36.9	33.1

Sample Preparation

The samples were prepared with phosphorus pentoxide (98.0% pure, purchased from Aldrich), filtered deionized water (purchased from Fischer Scientific) and deuterium oxide (99.9 atom % D, purchased from Aldrich). Six samples with ratio R=1.5, 2.0, 2.5, 3.0, 4.0, 5.0 were prepared, each in deuterated and hydrogenated water.

P_2O_5 is highly hydrophilic, and great caution has to be taken in order to avoid contamination of the sample by exposure to humidity in the atmosphere. Initially a certain amount of P_2O_5 was measured in a glove box filled with dry Argon gas. The samples were then exposed to H_2O or D_2O in a hydration chamber for 96 hours. Finally the weight was measured and appropriate amounts of H_2O and D_2O were added using a micropipette. The samples had to be prepared by slowly hydrating P_2O_5 in order to avoid an uncontrollable exothermic reaction. To ensure uniformity, the samples were stirred at 180℃ for 45 minutes immediately after completion of the measuring process.

Broadband dielectric Spectroscopy (BDS), Differential Scanning Calorimetry (DSC) and Brillouin Light Scattering (BLS) were performed on these sets of samples. In order to insure accuracy of sample preparation, dielectric measurements of the samples with ratio R=1.5 and R=5 were compared to equivalent concentrations of purchased phosphoric acid solutions 116 wt.% H_3PO_4 (Sigma-Aldridge) and 85 wt. % H_3PO_4 (Sigma-Aldridge), and 85 wt. % D_3PO_4 (Sigma-Aldridge). The results of BDS measurements of prepared and purchased samples coincided, implying that the sample preparation via hydration of P_2O_5 was successful.

In addition to the above-mentioned samples, more diluted samples with ratio R=7.0, 9.0, 14.0 were prepared for both isotopes. These samples were prepared by adding calculated

amounts of H_2O and D_2O to 85 wt.% H_3PO_4 and D_3PO_4, respectively. These more diluted samples were only measured using DSC.

Measurement Techniques

Proton conductivity is related to dielectric properties such as permittivity, conductivity and electric modulus. These properties can be measured using broadband dielectric spectroscopy. Temperature dependence of dielectric properties also provides information about the glass transition. To further investigate T_g, differential scanning calorimetry and Brillouin light scattering is used to determine the temperature dependence of heat capacity and sound velocity within the sample. The following section provides a detailed discussion of the measurement techniques used in this study.

Broadband Dielectric Spectroscopy

Dielectrics are materials, which can be polarized by an electric field. This polarization is exhibited by rearranging of dipolar molecules, and electron clouds. Charges are attracted to the opposing polarity of the electric field, causing negative charge to be drawn towards the cathode and positive charge drawn towards the anode. Broadband dielectric spectroscopy (BDS) studies the frequency dependence of the dielectric relaxation processes over a broad frequency band of 10^{-6} Hz to 10^{7} Hz.

BDS measures a samples impedance, Z, in response to the applied electric field $E(\omega)$ with frequency ω. Dielectric data provide information about complex conductivity, σ^*, complex permittivity, ε^*, complex dielectric modulus, M^*, and other dielectric properties of the sample. In

order to interpret these quantities, it is important to first understand their relation, and physical meaning. Further examination of the theory of dielectric spectroscopy is provided in the following section.

When an external electric field is applied to a dielectric material it displaces internal electric charges, causing a polarization effect. The dielectric displacement of charges, $\boldsymbol{D}$, occurs in forms of molecular reorientation of dipolar molecules, charge drift, or translational diffusion of mobile charge carriers such as electrons or ions. $\boldsymbol{D}$ of a dielectric media is related to the external electric field, $\boldsymbol{E}$, via the permittivity of free space, ε_0, and the permittivity of the material, ε^*.

$$\boldsymbol{D} = \varepsilon^* \varepsilon_0 \boldsymbol{E} \qquad \textit{eq. 3.2}$$

Permittivity is a measure of resistance of a material to an applied electric field. The dielectric permittivity, or complex dielectric function, is frequency dependent when a periodic alternating electric field of the form $\boldsymbol{E}(t) = E_0 e^{-i\omega t}$ is applied. The frequency dependent complex permittivity, $\varepsilon^*(\omega)$, is then defined in terms of its real, $\varepsilon'(\omega)$, and imaginary, $\varepsilon''(\omega)$, components as follows.

$$\varepsilon^*(\omega) = \varepsilon'(\omega) - i\varepsilon''(\omega) \qquad \textit{eq. 3.3}$$

$\varepsilon'(\omega)$ is proportional to the energy stored reversibly in the system, while $\varepsilon''(\omega)$ is proportional to the energy which is dissipated by the system, per period of oscillation of the electric field. Polarization on a macroscopic level consists of the summation of microscopic dipoles per volume, and the induced polarization of the external field. The polarization, $\boldsymbol{P}$, is defined using the difference in dielectric displacement in a dielectric and vacuum, and can also be expressed in terms of $\boldsymbol{E}$ as follows.

$$\boldsymbol{P} = \boldsymbol{D} - \boldsymbol{D}_0 = (\varepsilon^* - 1)\varepsilon_0 \boldsymbol{E} = \chi^* \varepsilon_0 \boldsymbol{E} \qquad \textit{eq. 3.4}$$

$\boldsymbol{D}_0$ refers to the displacement caused by an electric field in the absence of the dielectric media. χ^* is the dielectric susceptibility, which indicates the degree of polarization of a material.

When taking Ohm's Law, eq. 3.5, into account, a relationship between current density, $\boldsymbol{j}$, and the electric field can be established using complex conductivity, $\sigma^*(\omega) = \sigma'(\omega) + i\sigma''(\omega)$. Complex conductivity is frequency dependent and consists of real, σ', and imaginary, σ'', conductivity components.

$$\boldsymbol{j} = \sigma^* \boldsymbol{E} \qquad \textit{eq. 3.5}$$

Faraday's law, $\nabla \times \boldsymbol{E} = -\frac{\partial}{\partial t}\boldsymbol{B}$, states that the curl of the electric field is equivalent to the negative change in the magnetic field, **B,** with time. This law describes how a time variant magnetic field creates an electric field. Using Faraday's law, the displacement field, eq. 3.2, and the Ohm's law, eq. 3.5, a relationship between complex conductivity and complex permittivity can be established as follows. In this case we are not considering a magnetic field so $\nabla \times \boldsymbol{H} = 0$.

$$\mathbf{0} = \sigma^* \boldsymbol{E} + \varepsilon_0 \varepsilon^* \frac{\partial}{\partial t}\boldsymbol{E} \qquad \textit{eq. 3.6}$$

$$\sigma^* \boldsymbol{E} = -\varepsilon_0 \varepsilon^* (-i\omega)\boldsymbol{E} \qquad \textit{eq. 3.7}$$

$$\sigma^* = i\omega\varepsilon_0\varepsilon^* \qquad \textit{eq. 3.8}$$

Complex conductivity and complex permittivity are different electrical properties that can be related using $i\omega\varepsilon_0$.

Dielectric data can also be represented in terms of the dielectric modulus. The complex dielectric modulus, M^*, corresponds to the decay of the electric field under constant dielectric displacement and is inversely related to complex permittivity.

$$M^* = \frac{1}{\varepsilon^*} \qquad \textit{eq. 3.9}$$

The complex dielectric modulus consists of real, M', and imaginary, $M"$, components as $M^*(\omega) = M'(\omega) + iM"(\omega)$. These can be represented in terms of permittivity.

$$M'(\omega) = \frac{\varepsilon'(\omega)}{\varepsilon'^2(\omega) + \varepsilon"^2(\omega)} \qquad eq.\ 3.10$$

$$M"(\omega) = \frac{\varepsilon"(\omega)}{\varepsilon'^2(\omega) + \varepsilon"^2(\omega)} \qquad eq.\ 3.11$$

The modulus representation can be advantageous when measuring ionic conductors due to the insensitivity to electrode polarization (EP). When a low frequency external electric field is applied to the sample, free charge carriers such as ions accumulate at the surface of the electrodes. This causes a resistive layer at the sample-electrode surface. Polarization due to ion diffusion is reversible when the external field is removed, causing an effect in real permittivity. M" is mainly influenced by ε", meaning that it is rather insensitive to electrode polarization. The imaginary component of the dielectric modulus is therefore helpful in analyzing ionic conductivity without the influence of electrode polarization. In order to measure the dielectric properties, BDS uses a cell geometry in which the sample is contained between two parallel electrodes. Electric characteristics of the cell resemble that of a parallel plate capacitor. The system can then be modeled as a resistor-capacitor (RC) series circuit as shown in Figure 3.2. An electric potential, V_1, is applied by a voltage generator. This sinusoidal potential generates the electric field across the sample. The second potential V_2 is determined via the current I across the resistor R. Voltage, current and resistance are related using Ohms law $V = IR$ in a direct current application. In alternating current applications the phase difference, ϕ, between the voltage $V(t) = V_{max}\cos(\omega t)$, and the current, $I(t) = I_{max}\cos(\omega t + \phi)$, has to be taken into account. The complex impedance, $Z^*(\omega)$, of the sample can then be calculated using the electric potential

across the capacitor and the resistor and the current flowing throughout the system $V_1^*(\omega)$, $V_2^*(\omega)$, and $I^*(\omega)$, respectively.

$$Z^*(\omega) = \frac{V_1^*(\omega)}{I^*(\omega)} = R\left[\frac{V_1^*(\omega)}{V_2^*(\omega)} - 1\right] \qquad eq.\ 3.12$$

Once the complex impedance of the sample is measured, complex permittivity can be derived using the impedance formula of a capacitor $Z^* = \frac{1}{j\omega C^*}$, and the complex dielectric function of a capacitor $\varepsilon^*(\omega) = \varepsilon'(\omega) - i\varepsilon''(\omega) = \frac{C^*(\omega)}{C_0}$. Here the complex capacitance of the sample and the capacitance of vacuum are symbolized by $C^*$and C_0, respectively. The complex dielectric function in terms of complex impedance is then given by

$$\varepsilon^*(\omega) = \frac{1}{i\omega Z^*(\omega) C_0} \qquad eq.\ 3.13$$

All other necessary quantities such as complex conductivity, complex modulus, and their respective real and imaginary contributions can then be derived using the complex permittivity as shown above.

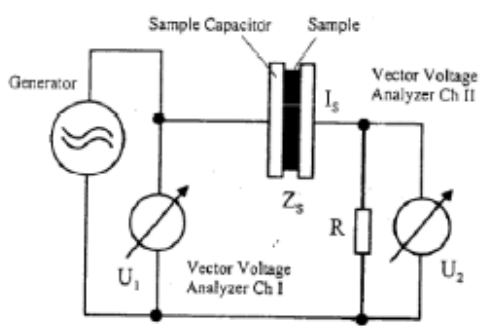

Figure 3.2 Schematic of Novocontrol alpha analyzer used to measure the impedance of the sample Z_s. The potentials U_1 and U_2 as well as a resistance R are used to measure Z_s [41].

Dielectric measurement

In this research, measurements were conducted using a dielectric spectrometer (Novocontrol alpha analyzer) in a frequency range of 10^{-2} to 10^{7} Hz. The dielectric sample cell consists of round electrodes in a parallel plate capacitor set up. Top and bottom electrodes were separated using a Teflon spacer, creating a cylindrical sample volume with a radius of 19mm and a thickness of 0.9mm. The cell design is specifically chosen to minimize electrode polarization by reducing the thickness of the polarization layer with respect to that of the total sample thickness. Gold plated electrodes were used to reduce interaction with the concentrated acids. Special precautions were taken since the highly ordered atomic structure of gold can cause surface induced crystallization of the sample. In order to erase thermal history of the sample, the loaded cell was held at 80^{0}C for 10 minutes prior to quenching to the initial temperature of the measurement. The sample temperature was equilibrated for 20 minutes after each temperature change.

The drawback of BDS is the difficulty of determining the origin of a relaxation processes. Dielectric data alone does not clarify if a relaxation process corresponds to motion of an electric dipole, molecule, or part of molecule. Furthermore, non-dipolar molecules are not responsive to the external field and so don't appear in the measurement. BDS can however be a powerful tool when used in conjunction with complimentary experiments such as light scattering spectroscopy.

Differential Scanning Calorimetry

Differential Scanning Calorimetry (DSC) is a measurement technique, which determines the amount of heat that is required to change the temperature of the sample. Thermodynamic

processes such as transitions of phase or state of a sample absorb or release thermal energy and can so be measured using DSC. The heat capacity of a sample, C_p, is a measure of the amount of heat, q, required in order to change the temperature, T, by a certain amount.

$$C_p = \frac{dq}{dT} = \frac{change\ in\ heat}{change\ in\ temperature} \qquad eq.\ 3.14$$

Transitions between solid, liquid, and gaseous phases are thermodynamic processes that require a transfer of energy. When a material is heated or cooled through a phase transition it either absorbs or releases thermal energy. Transition in which a sample absorbs heat such as melting or evaporating are referred to as endothermic. The reverse process releases heat from the sample and is referred to as exothermic. Exothermic processes include crystallization or oxidation. During a phase transition the amount of thermal energy required to alter a sample's temperature changes due to the partial release or absorption of energy by the transition. This causes a measurable change in C_p of the sample during a transition.

$$Heat\ flow = \frac{dq}{dt} \qquad eq.\ 3.15$$

$$Heating\ rate = \frac{\mathrm{d}T}{dt} \qquad eq.\ 3.16$$

Differential scanning calorimetry compares the amount of heat absorbed or released by a sample with that of an empty reference pan. C_p is calculated from the difference in temperature response of the cell filled with a known amount of sample and that of the empty reference pan. Typically, DSC results are presented as heat flow as a function of temperature. Figure 3.3 shows a representation of the heat flow of different thermodynamic processes versus temperature. Crystallization and melting are indicated as exothermic and endothermic processes, respectively.

The glass transition is not a true phase transition but rather a change in local degrees of freedom of the molecules. Molecular motion is frozen in the glassy state. Heating across T_g,

appears as an endothermic step in heat flow. The midpoint of the glass transition can be found using derivative analysis. The temperature of the peak position of the derivative of heat flow with respect to temperature indicates the maximum change in heat flow. This maximum occurs at the midpoint of the Glass transition. The details of measurement are discussed in the following section.

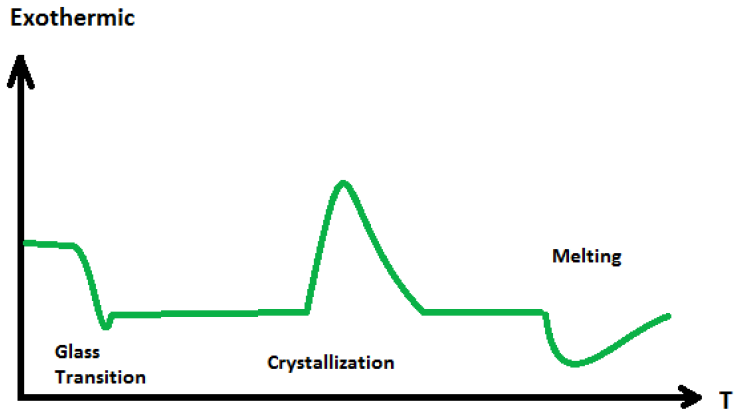

Figure 3.3 Heat flow into a material is depicted upon heating. Temperature range from glassy to molten state. Thermodynamic processes of a material, such as glass transition, crystallization and melting are depicted.

DSC Measurement

The measurement was conducted using a TA-Instruments Q1000 Differential scanning Calorimeter. The samples were contained in 50µl stainless steel cylindrical pans with an o-ring seal and a lid. The sample was loaded into the cell via micropipette and weight to determine the exact amount of sample. The cell was then hermetically sealed using a special T-Zero press. All

cell components were purchased from TA Instruments. During the measurement, the samples were held under filtered nitrogen atmosphere to avoid crystallization of moisture introduced through humidity in the atmosphere. In order to properly compare the glass transition to that of the dielectric data, the sample was equilibrated at 80°C for five minutes prior to starting the temperature cycle. The samples were then cooled to a temperature in access of 30°C below the glass transition, and kept isothermal for 5 minutes to ensure thermal equilibrium. The measurements were conducted on the heating cycle at a rate of 5°C/min. Structural changes as a function of temperature can also be investigated using light scattering measurements, as discussed in the following section.

Brillouin Spectroscopy

Brillouin light scattering (BLS) is a technique, which measures the frequency shift of light due to inelastic scattering. Such scattering is caused by propagation of sound waves through a media. The velocity of sound propagation is related to the rigidity of the material. Material properties such as rigidity are temperature dependent. Hence BLS measurements can provide information about the different structural properties of a sample at different temperatures. The details of BLS are described in the following section.

Light, which impacts a particle much smaller than the wavelength of the light, can create an electric dipole moment. The radiation given off by this oscillating dipole is called scattered light. The scattered wave vector, $\boldsymbol{q}$, is the difference of the incoming, $\boldsymbol{k}_i$, and scattered, $\boldsymbol{k}_f$, wave vectors. Figure 3.4 shows a graphic representation of eq. 3.17.

$$\boldsymbol{q} = \boldsymbol{k}_f - \boldsymbol{k}_i \qquad \textit{eq. 3.17}$$

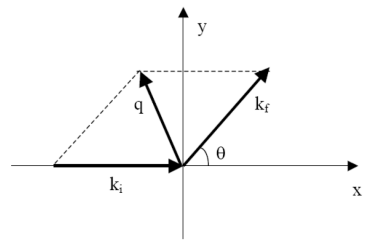

Figure 3.4 The interaction of incoming wave vector, $\boldsymbol{k}_i$, and refracted wavevector, $\boldsymbol{k}_f$, result in the scattered wave vector $\boldsymbol{q}$. The scattering angle is indicated by θ [42].

The energy of light is slightly altered during the scattering process, which can be observed due to slight changes in frequency of the light. This change of energy is negligibly small, and so conservation of energy $|\boldsymbol{k}_f| = |\boldsymbol{k}_i|$, can be assumed. The scattered wave vector can be expressed in terms of, the refractive index of the sample, n, the wavelength of light, λ, and the angle of scattered light, θ. The symbol $|\ |$ represents the magnitude of the vector.

$$|\boldsymbol{q}| = 2\pi|\boldsymbol{k}_i| sin\left(\frac{\theta}{2}\right) = \frac{4\pi n}{\lambda} sin\left(\frac{\theta}{2}\right) \qquad \textit{(eq. 3.18)}$$

Rotational and translational motion of the dipole can alter the frequency and intensity of the admitted light. Light can scatter elastically, quasi-elastically, and in-elastically. These three types of scattering are briefly discussed below. Figure 3.5 shows a sketch of light scattering intensity as a function of the frequency shift, $\Delta\omega$, based on the different types of scattering. The scattered wave can have an increase or decrease of frequency relative to the frequency of the incoming light. This creates a symmetric plot centered on the $\Delta\omega = 0$. Elastic scattering, also called Rayleigh scattering, conserves energy, leaving the frequency of the scattered light unchanged from the incoming light. This unchanged frequency presents itself as the central peak at $\Delta\omega = 0$ in Figure 3.5 and provides information about the static structure of a sample.

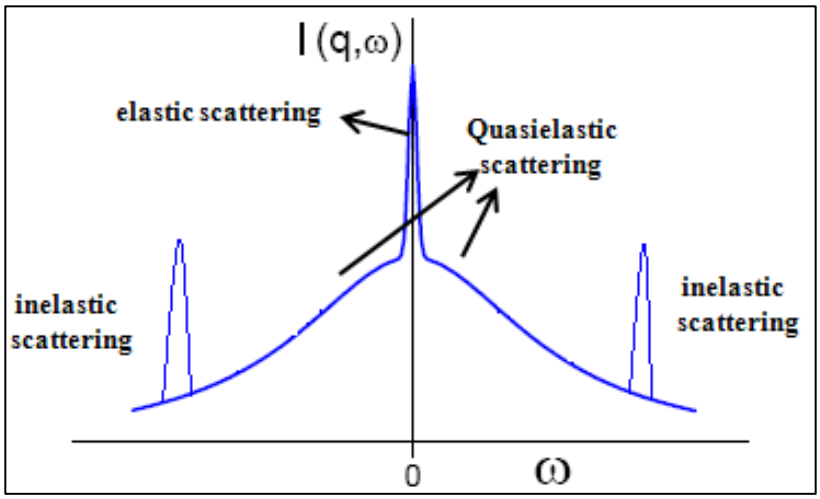

Figure 3.5 Schematic of elastic, quasi-elastic, and inelastic light scattering as a function on change of frequency [42].

The second type of scattering is the Quasi-elastic scattering, or Rayleigh wing, which refers to the broadening of the central peak due to the change of frequency from elastic scattering. This scattering is caused by rotational and translational relaxation of molecules. These processes interfere with the oscillation of the electric dipole. Altering the dipole oscillation affects the radiated light and causes a broadening of the central peak. Hence, the amount of broadening provides information about molecular motion within the sample. The third type of scattering is inelastic scattering. It is caused by the influence of vibrational modes consisting of localized and propagating motion of molecules. Localized motion is independent of ***q***, while propagating motion exhibits ***q*** dependence. The latter can be induced by transverse and longitudinal waves, which can stem from optical and acoustic origin. Inelastic scattering presents itself with a distinctive intensity peaks. Inelastic scattering caused by transverse and longitudinal waves can be measured using Raman and Brillouin spectroscopes for the higher frequency optical modes

(THz region) and the lower frequency acoustic modes (GHz), respectively. Both techniques are used to study vibrational and rotational modes of a sample. Within this study, light scattering techniques are used to determine the temperature dependence of material properties of phosphoric acid samples. Therefore further discussion of light scattering will focus exclusively on BLS. Utilizing Brillouin light scattering, the sound velocity in a sample v can be calculated from the peak frequency of the Brillouin shift f, as well as the wave vector of the scattered beam $\boldsymbol{q}$. The wave vector can be expanded using the expression eq. 3.15.

$$v_L = f\frac{2\pi}{\boldsymbol{q}} = \frac{\lambda f}{2nsin\left(\frac{\theta}{2}\right)} \qquad eq.\ 3.19$$

Material properties e.g. the longitudinal elastic modulus M can be derived using density ρ, and the longitudinal sound velocity, v_L, of the sample.

$$M = \rho v_L^2 \qquad eq.\ 3.20$$

The elastic modulus is a measure of mechanical response of a sample as a result of applied force. The modulus is temperature dependent since rigidity of molecular structure usually increases upon cooling. Increase in elastic modulus causes an increase in sound velocity, which in turn causes an increase in frequency shift of the Brillouin peak. Figure 3.6 shows the raw light scattering data of the deuterated phosphoric acid sample with concentration R=5. A clear shift of the Brillouin peak is observed at temperatures ranging from 270K to 170K. $\Delta\omega$ increases with decreasing temperature. It has already been determined in chapter 2 that temperature dependence of material properties differs when a sample is cooled from a liquid into a glassy state. The change of temperature dependence of the Brillouin peak frequency is observed upon vitrification. From this the glass transition temperature of the sample can be determined using Brillouin light scattering.

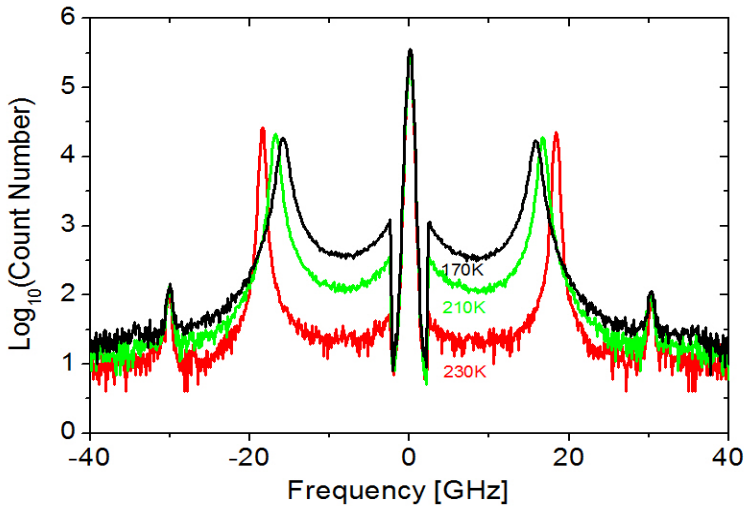

Figure 3.6 Raw Brillouin scattering data of a deuterated phosphoric acid sample with concentration R=5. Temperatures 170K, 210K, and 230K are shown in black, green and red, respectively.

Brillouin Measurement

Scattered light was measured using a tandem Farby-Perot interferometer (Sandercock Model). The incoming green laser had a wavelength of 532nm. Samples were contained in 1ml cylindrical glass vials, which were extensively rinsed and dried prior to loading of the sample to avoid impurities. The deuterated and hydrogenated phosphoric acid samples with concentration R=5 were filtered into the sample vial using a 22μm syringe filter. High viscosity of the samples with concentration of R=1.5 prohibited filtering and so were measured unfiltered. The following chapter will discuss the results obtained by measurement techniques described above.

CHAPTER 4:

RESULTS AND DISCUSSION

The glass transition and dielectric properties of deuterated phosphoric acid are discussed in the following chapter. Isotope effects become visible when compared with hydrogenated phosphoric acid. In the following chapter, these effects will be discussed from a classical and quantum mechanical view.

Dielectric Data of Deuterated Phosphoric Acid

An example of raw dielectric spectra of hydrated phosphoric acid of concentration R=1.5 at temperatures ranging from $-60°C$ to $-30°C$ are shown in Figure 4.1. Here the real part of dielectric permittivity ε', the imaginary dielectric modulus M'', and the real part of electric conductivity σ' are plotted versus frequency in a), b), and c), respectively. Ionic conductivity appears as a process in ε', as a peak in M'', as well as the onset of frequency dependence of σ'. The conductivity relaxation time τ_σ was derived from the M'' spectra as opposed to ε', due to its immunity to electrode polarization, as explained in the previous chapter. For the concentration R=1.5, the peak frequency of ionic conductivity moves from roughly 0.5Hz to 3000Hz with increase in a temperature of $30°C$. To avoid crystallization the sample was quenched below T_g and measured upon heating. Data collected while heating and cooling of the sample were consistent, indicating reproducibility of the experimental data. One important characteristic of the glass transition temperature is the change of temperature dependence of the dielectric properties. The temperature dependence of the sample becomes much weaker below the glass transition due to freezing in a non-equilibrium state.

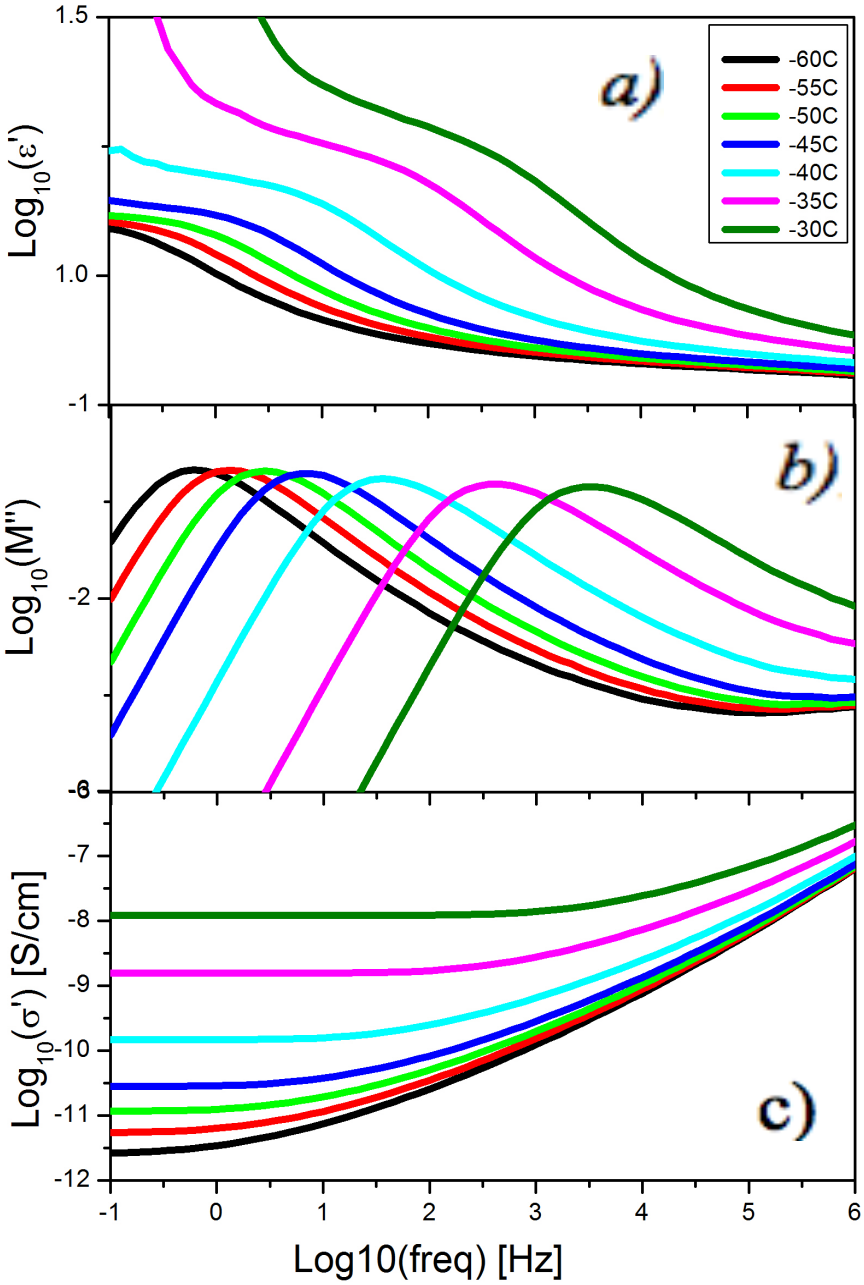

Figure 4.1: Dielectric permittivity ε', imaginary dielectric modulus M'', and the real part of electric conductivity σ' of $P_2O_5(1:1.5)D_2O$ are plotted versus frequency in the top, center and bottom part respectively. The depicted temperatures range from $-60°C$ to $-30°C$ in increments of $5°C$.

To analyze the temperature dependence of ionic conductivity in more detail, the conductivity relaxation time τ_σ of M'' and the DC conductivity plateau σ_τ of a broad range of acid concentrations can be represented in Arrhenius plots. These representations can highlight a clear change in the temperature dependence of both, τ_σ and σ_τ, at the glass transition. In the glass phase region below T_g, structural dynamics of the phosphorus-pentoxide deuterium mixture is essentially arrested, limiting ionic conduction to intermolecular hopping motions. This retardation of intermolecular structural diffusion is the cause of the alteration in temperature dependence of ionic conductivity. The remainder of this chapter is devoted to the discussion of such phenomena.

Glass Transition in Dielectric Spectroscopy

In this case, glass transition is determined from the temperature dependence of τ_σ, where the glass transition of all ratios is measurable, while only a limited experimental window is available in σ_τ. Conductivity relaxation time decreases with temperature as seen in Figure 4.2. Here τ_σ of deuterated phosphoric acid with ratios R=1.5, 2, 2.5, 3, 4, 5 are displayed in Figure 4.2 a), while the deuterated acids are compared to their hydrogenated counterparts in Figure 4.2 b). Above T_g the Super-Arrhenius behavior of τ_σ can be described using the Vogel-Fulcher-Tammann (VFT) equation eq. 2.2. Below the glass transition temperature, conductivity behaves as an activated process and follows the Arrhenius equation. The intersection point of these two different regimes marks the midpoint of the glass transition, which is the initial focus of this chapter. Characteristics of the fitting functions as well as concentration dependence of τ_σ will be discussed in further detail in the second part of the chapter.

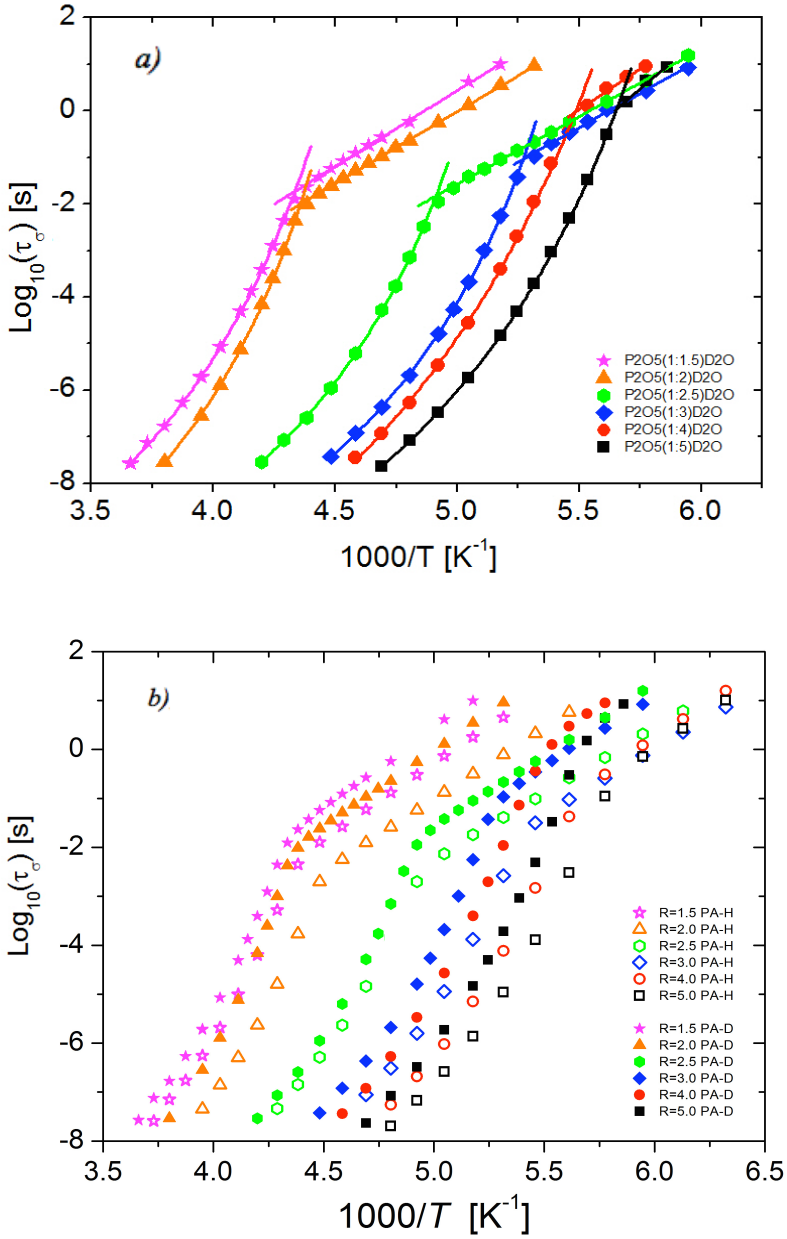

Figure 4.2 Conductivity relaxation time τ_σ of deuterated phosphoric acid at different concentrations, a), and the comparison to the hydrated counter parts, b), shown in Arrhenius plots. The shown molar ratios correspond to R=1.5 (magenta star), R=2.0 (orange triangle), R=2.5 (green hexagon), R=3.0 (blue diamond), R=4 (red circle) and R=5 (black square) for the deuterated (closed) and hydrated (open) symbols respectively.

The glass transition temperature of concentrated phosphoric acids R=1.5 and R=2 is 230.7K and 229.5K for the deuterated, and 227.4 and 222.4K for the hydrogenated samples, respectively. With further dilution T_g decreases for samples of concentration R=3 (D_3PO_4 or H_3PO_4) to R=5 with 189.7K and 176.9K for deuterated and 185.3K and 172.1K for hydrogenated samples. For this measurement, concentration dependence of the glass transition temperature is expected due to the large difference in T_g of the individual components, D_2O, H_2O and P_2O_5 being 140K, 136K, and 590K respectively [27]. Hence, concentrated phosphoric acids are expected to display a higher glass transition temperature compared to the diluted regime. The mixtures used in the experiments approach the T_g's of the individual components at the diluted and concentrated regions. Measurements of low temperature dynamic properties of diluted systems using dielectric spectroscopy are challenging, since the ionic conductivity processes shift to lower frequencies, and moves outside of the measurable window. The glass transition temperature of PA was therefore further investigated using DSC to allow for a broader range in temperature and concentration.

Differential Scanning Calorimetry

In the DSC measurements, samples with ratios of R= 7, 9, 14 of P_2O_5 to both hydrogenated and deuterated water were measured, in addition to the R=1.5, 2, 2.5, 3, 4, 5 samples used in dielectric spectroscopy. T_g appears in the calorimetric temperature cycle on the cooling as well as the heating cycle. However only the heating cycle will be considered, in order to allow direct comparison to the Dielectric spectroscopy data.

Upon heating, the sample goes from the glassy into the liquid state, causing an initial spike in heat flow rate, followed by immediate enthalpic recovery to the liquid equilibrium state. Figure 4.3 shows the heating cycle of the raw DSC data, where the data were shifted vertically to clarify the behavior and highlight the change in the glass transition temperatures amongst the samples. The midpoint of the glass transition temperature was determined via peak position analysis of the derivative of the heat flow with temperature. The sample with the ratio R=3 crystalizes upon heating which is seen in the Figure 4.3 as a strong exothermic process.

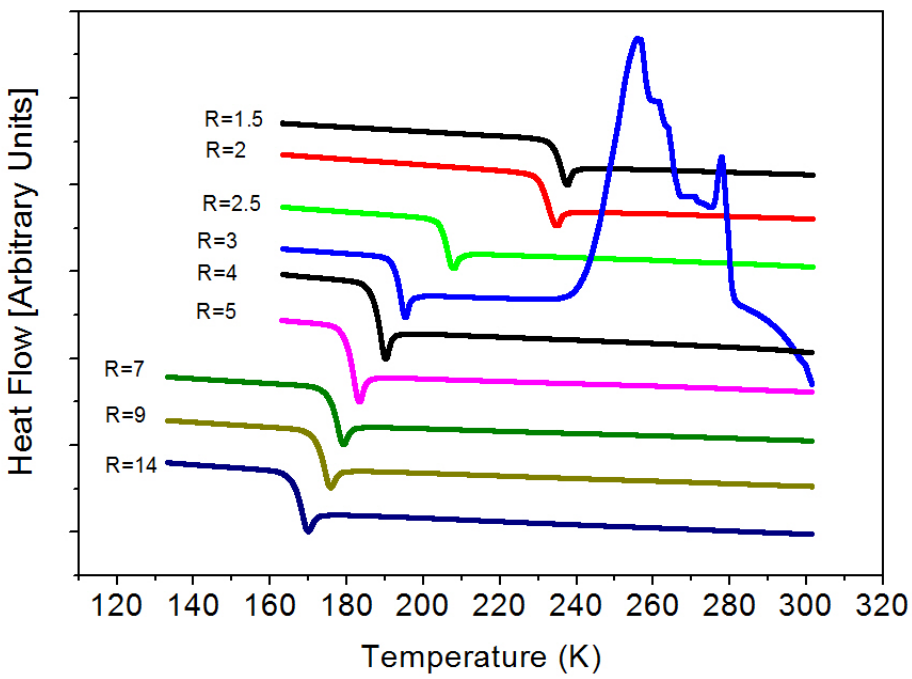

Figure 4.3 The heat flow of different concentrations of deuterated phosphoric acids as measured on the heating cycle via Differential Scanning Calorimetry (Exo Up). Various concentrations are indicated on the plot. T_g appears as an endothermic process. The sample with the ratio R=3 corresponds to neat phosphoric acid (D_3PO_4) which crystalized at around 273K.

T_g data for both deuterated and hydrated phosphoric acid were collected using DSC measurements and compared to literature values of Corti et al. [33] (black) and Aihara et al. [22] (green) in Figure 4.4. In this research, T_g values ranged from 236.0K to 181.8K for deuterated and from 233.5K to 178K for the hydrogenated phosphoric acid samples with R=1.5, 3, 5, respectively. Glass transition temperatures of hydrated phosphoric acid coincide with those collected by the group of Angell in the concentrated region. The T_g begins to diverge from Angell's data in the diluted regime. Similar to the dielectric measurements, the glass transition temperature of the deuterated sample is higher than that of the hydrogenated sample, and the difference in T_g increases with increasing water content. Aihara *et al* measured glass transition of a mixture of deuterated and hydrated phosphoric acid. As expected, the data falls in between that of pure hydrogenated and pure deuterated phosphoric acid.

Glass transition temperatures converge to a value which, when extrapolated to the dilute limit, can be hint to the T_g values of pure hydrogenated or deuterated water. It has been suggested by Angell et al. that the Gordon Tailor (GT) equation, eq. 2.8, can be used to fit such data. The Gordon Tailor equation did not produce a good description of the DSC data collected in our research. The GT equation proved insensitive to fitting parameters and could not fit diluted data accurately. Extrapolation to pure components leads to values in access of 145K and 155K for hydrated and deuterated water, respectively. These values are near 10K too high compared to the commonly accepted T_g values.

A higher glass transition temperature for the sample with concentration R=2 is observed. This is also apparent in the conductivity spectra as well as viscosity and NMR measurements [34] and can be accounted for by a change in bond structure, which is formed by P2O5 (1:2)

H2O. This phenomenon will be further discussed in the later section on conductivity relaxation time of these samples.

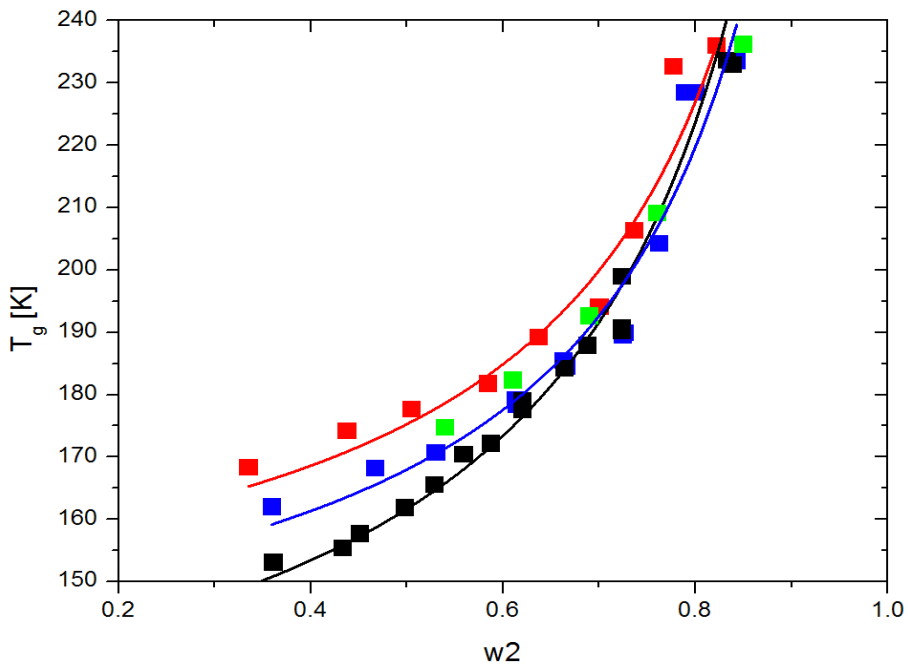

Figure 4.4 Glass transition temperatures of deuterated (red) and hydrogenated (blue) phosphoric acid are compared to data from literature Aihara et al. [22] (green) and Corti et al. [33] (black). T_g is plotted versus w_2 which is the weight fraction of P_2O_5 of the sample for easy extrapolation from zero to one. The lines indicate the Gordon Taylor fit for each data set corresponding to the color.

Brillouin Light Scattering

Measurements of the Glass transition temperature were further verified through Brillouin scattering measurements for selected ratio's R=1.5, 5. The Brillouin peak in light scattering

spectra corresponds to a Doppler shift in frequency, caused by propagating acoustic vibrations within the sample. The Brillouin peak freaquency as a function of temperature is presented in Figure 4.5 for both hydrogenated and deuterated samples. The deuterated samples exhibit a lower Brillouin frequency compared to their hydrogenated counterparts, as expected for the higher oscillating mass.

Furthermore, Figure 4.5 demonstrates a clear change in temperature dependence of the Brillouin frequency at the glass transition. Near linear temperature dependence is observed above and below the transition. The change in temperature dependence of the Brillouin frequency is caused by the changing velocity of sound propagation in the sample. The change in rigidity of the material lessens, when the sample is vitrified.

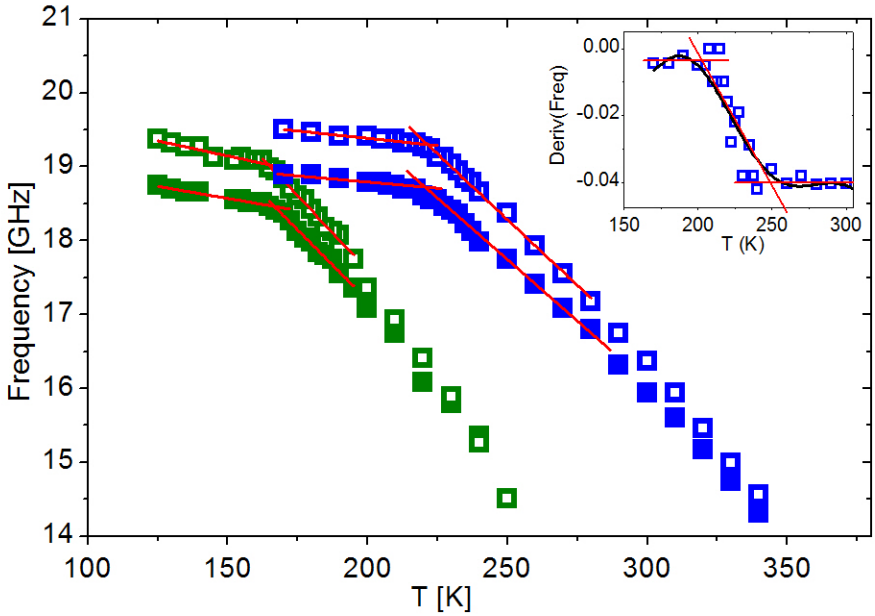

Figure 4.5 Average Brillouin frequency of deuterated (closed) and hydrogenated (open) phosphoric acid at R=1.5 (blue) and R=5 (green) plotted against temperature. The inset shows the derivative of frequency with temperature across the glass transition.

A more detailed description of the relationship between rigidity of the sample and change in frequency by inelastic scattering off of longitudinal wave motion is provided in the Brillouin light scattering section of chapter 3. The mid point temperature of the transition was determined by derivative analysis and smoothing of the data as demonstrated in the inset in Figure 4.5. Horizontal lines indicate linear temperature dependence above and below T_g, while the midpoint temperature was taken to be at the center of the transition. As in the DSC and Dielectric measurements the deuterated samples show a higher glass transition temperature. Due to excessive data manipulation, the error-bars of determining glass transition using this technique was within a few degrees, though a clear trend can be observed through internal consistency of the measurement itself.

Glass Transition - Discussion

To identify the isotope effect on the glass transition temperatures of phosphoric acid at different concentrations, a variety of experimental methods were utilized in this research. The comparison of the glass transition data of the three methods used (Figure 4.6) yields slight differences between experimental methods. Though all methods are internally consistent concerning the difference in glass transition temperature ΔT_g, some variance exists between the results of the different experimental techniques. Brillouin and Dielectric measurements yield lower glass transition temperatures than DSC. This difference in temperature can be explained by vast difference in heating and cooling rate during the measurements. Brillouin light scattering and dielectric measurements were conducted in temperature steps of 2.5k surrounding the glass transition, taking tens of minutes per temperature. DSC measurements were conducted with rates

of 5K/min. Due to the fact that the glass transition is a broad transition, the fast heating rate of DSC led to higher indicated T_g than the slow heating and cooling rate of the other two methods, resulting in the difference visible in Figure 4.6. Nevertheless, this research aimed to identify the isotope affects in the glass transition temperatures of $D_2O - H_2O$ of different acid concentrations.

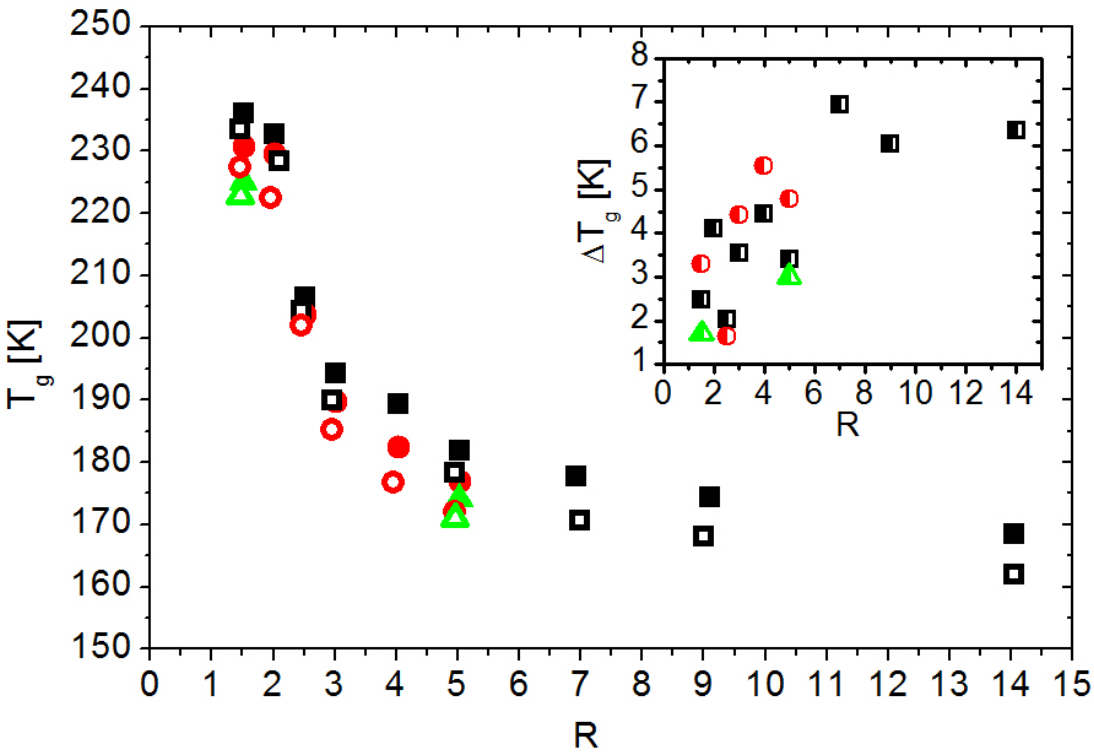

Figure 4.6 Comparison of glass transition temperatures obtained using DSC (black squares), dielectric spectroscopy (red circles) and Brillouin light scattering (green triangles). Deuterated and hydrogenated samples are represented by closed and open symbols, respectively. The insert shows the difference in the glass transition temperatures ΔT_g between deuterated and hydrogenated samples with half filled symbols of the same color scheme.

The differences between outcomes of the previously described methods used are of insignificant importance for this research. As displayed in Figure 4.6, the measurements show that the T_g of D_2O – containing samples is always greater than that of H_2O - containing ones, and the difference increases with R. This difference in the glass transition temperature increases with water content. The results indicate that the difference in T_g between the heavier isotope D_2O and the lighter isotope H_2O is at least 6K. Variations in the data and accuracy of the Tg estimates complicate the determination of an exact extrapolation of ΔT_g between the two pure isotopes of water, but the data suggests that it is in the region of 6-8K. This value is higher compared to values suggested by extrapolating T_g of other proton conducting materials like $LiCl$ and $ZnCl_2$[27]. Consequently the results of this paper indicate that the isotope effect on glass transition is stronger than described by previous research. Our estimates for the isotope shift of Tg in water is consistent with *ΔTg*~10K revealed recently in studies performed in our gorup [26].

Proton Conduction and Conductivity Relaxation Time

Now that we have discussed the isotope effect in the glass transition, the question remains how the isotope effect impacts the proton conductivity. In order to study the isotope effect on proton conduction, let's go back to Figure 4.2, which presents the conductivity relaxation time of deuterated phosphoric acid. As previously demonstrated [34], the temperature dependence of dielectric data severely changes at the glass transition. τ_σ and σ_τ both exhibit a crossover from Super-Arrhenius to Arrhenius temperature dependence. Since ionic transport is no longer supported by structural relaxation and molecular diffusion (both are frozen below Tg), ionic motion most probably takes place through "Grotthuss type" hopping of protons. In this

case, the isotope effect should play a strong role in conductivity due to the mass difference of the proton and deuterium. The known change in mass difference in combination with the measurable change in conductive behavior can lead to a better understanding of the method of proton motion, which is discussed in the following section.

In order to determine dynamics below the glass transition, it is important to analyze the characteristics of ion conduction at T_g. Figure 4.7 shows the previously mentioned τ_σ data for deuterated phosphoric acid vs inverse temperature normalized by T_g. This representation emphasizes the difference in conductivity relaxation times at the glass transition between the samples.

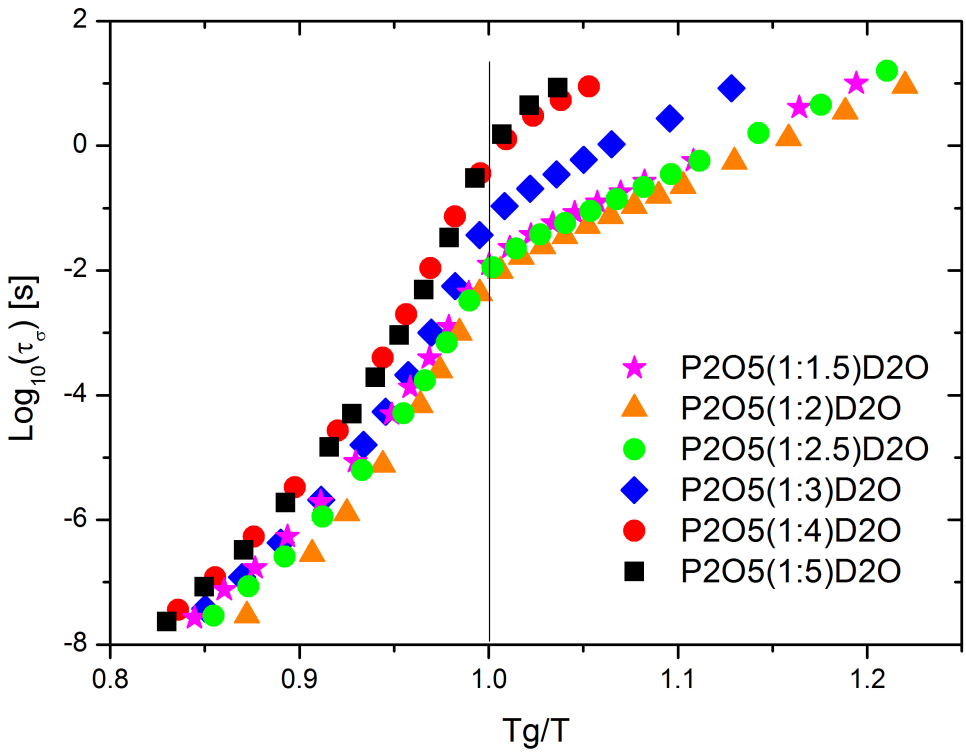

Figure 4.7Log$_{10}$ of conductivity relaxation time τ_σ of deuterated phosphoric acid at different water concentrations vs inverse temperature normalized to their Tg.

It is important to notice that τ_σ at T_g spans a range of over two orders of magnitude and does not increase monotonously with water concentration. Furthermore the hydrogenated phosphoric acid samples, show similar behavior shifted to faster time scales. To clarify, the conductivity relaxation times at the glass transition of each ratio are presented in Figure 4.8. The ratio of R=5 is excluded from the analysis in this section due to an inadequate amount of data points below the glass transition in the experimental window.

The conducted measurements show that the hopping time of ion conduction at T_g increases with dilution from $9.88\times10^{-3}s$ at R=2 to $9.02\times10^{-1}s$ at R=4, and $3.16\times10^{-3}s$ at R=2 to $1.26\times10^{-1}s$ at R=4 for the deuterated and hydrogenated phosphoric acid samples, respectively. At the R=1.5 ratios however the observed ion motion slows to $1.87\times10^{-2}s$ and $6.31\times10^{-3}s$ for deuterated and hydrogenated samples respectively. In this representation low values of τ_σ resemble fast ion jumps, which are desired in good proton conductors. The collected data suggests that ions transfer at a faster rate in more concentrated acids, reaching optimum at R=2, while increasing amount of water slows the process at Tg by near two orders of magnitude. The structures of phosphoric acid display strong concentration dependence. The time scale of ion hopping reaches a minimum when twice as many water molecules are present compared to phosphorus pentoxide. This suggests that the ratio of R=2 is favorable for the fast ion transport.

In order to analyze the impact of the isotope effect on ionic motion, the ratios of $\tau_\sigma(D)$ to $\tau_\sigma(H)$ at their Tg's were compared versus molar ratio in the insert in Figure 4.8. In this representation the data show a clear increasing trend with concentration ranging from a factor of 3 for R=1.5 to larger than 7 for R=4.

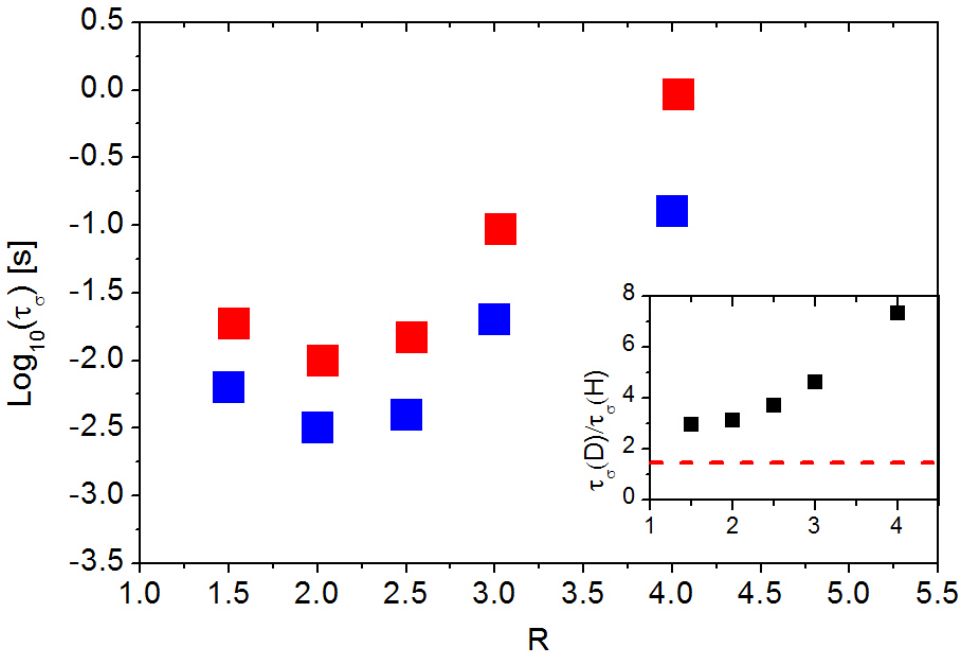

Figure 4.8 Log_{10} of conductivity relaxation time at the glass transition of deuterated (blue square) and hydrogenated phosphoric acid (red square). The insert shows the ratio of the above $\tau_\sigma(D)/\tau_\sigma(H)$ at their Tg's vs concentrationR. The expected value of $\sqrt{2}$ is indicated by a red dashed line.

In a purely classical model the ratio of time scale of ion transport should be constant, and equivalent to $\sqrt{M_D/M_H} = \sqrt{2}$ across all ratios, as per eq. 2.4, and various other models [43, 44]. The classical prediction is indicated on the plot by a red dotted line. Our measurements (Figure 4.8) show that even the minimum value of the ratio of relaxation times at R=1.5 is near twice of the expected value of the classical prediction, and the isotope effect only increases with molar amount of water in the sample. This is yet another indication [18-22] that the classical theory is not valid for ion transport, and further modification of the classical theory needs to be taken into consideration.

Molecular dynamics are frozen in the glassy state, causing ion transport to become an activated process below T_g. A certain activation energy E_A is now required in order to initiate ionic motion, which can be determined from the Arrhenius fit of τ_σ in Figure 4.2. Figure 4.9 shows the activation energies of deuterated (red) and hydrogenated (blue) phosphoric acids as determined from the Arrhenius fit at T<Tg. The activation energies within the measured set of ratios shows a distinct U-shape with a minimum centered on R=2.5. The activation energies decline from 62.2 $\frac{kJ}{mol}$ and 58.7 $\frac{kJ}{mol}$ at R=1.5 to 55.6 $\frac{kJ}{mol}$ and 51.4 $\frac{kJ}{mol}$ for R=2.5 for the deuterated and hydrogenated samples, respectively.

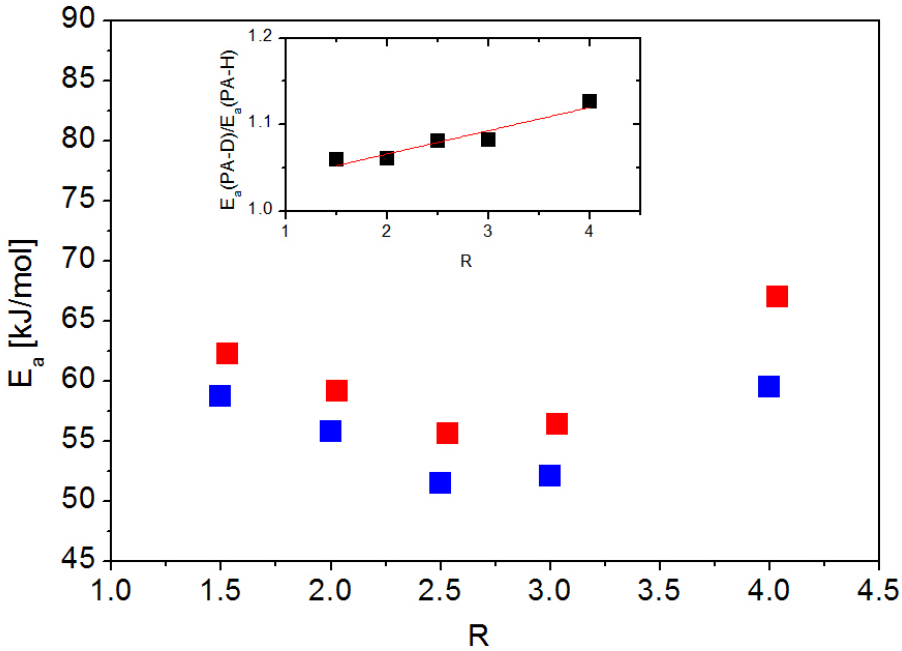

Figure 4.9 Activation Energies of ion conductivity in deuterated (red) and hydrogenated (blue) Phosphoric acid extracted from the Arrhenius fit of τ_σ at T<Tg. A minimum in Ea is observed in both cases at R=2.5. The insert shows the ratio of the activation energies for deuterated and hydrogenated samples.

Past the minimum, the activation energy increases to $67.0\,\frac{kJ}{mol}$ and $59.5\,\frac{kJ}{mol}$ at R=4.0. Therefore the energy barrier for a proton jump is less for the sample with R=2.5 than for highly dilute or highly concentrated regions. This is in approximate agreement with earlier findings of τ_σ and indicates favorable structures of ion conductivity at certain concentrations of phosphoric acid. Another important finding is that the activation energy of the deuterated samples is always higher than their hydrogenated analogs. To further analyze this phenomenon the ratio of activation energies of deuterated to hydrogenated phosphoric acid is shown in the insert of Figure 4.9. Across the sample range the ratio of the activation energies increases linearly by 6% from 1.06 to 1.13.

DC. Conductivity

In order to analyze the dynamics of ion motion above the glass transition it is best to focus on DC conductivity, due to a broader data range at higher temperatures. The temperature dependence of DC conductivity σ_τ, in different samples of deuterated phosphoric acid was obtained by tracking the DC plateau of the real part of conductivity with temperature (*Figure 4.10*). Conductivity increases with temperature as well as with increasing water content in the sample. The conductivity of deuterated phosphoric acid is always lower than that of the hydrogenated counterpart. At 50℃, which is equivalent to $3.09\ \frac{1000}{K}$ on the graph, σ_τ ranges from $2.13\times10^{-3}\,\frac{S}{cm}$ and $3.65\times10^{-3}\,\frac{S}{cm}$ at R=1.5 to $9.25\times10^{-2}\,\frac{S}{cm}$ and $1.71\times10^{-1}\,\frac{S}{cm}$ for R=5 for deuterated and hydrogenated samples, respectively. Hence the conductivity in the high temperature region is roughly 50% higher in the hydrated samples than in the deuterated ones.

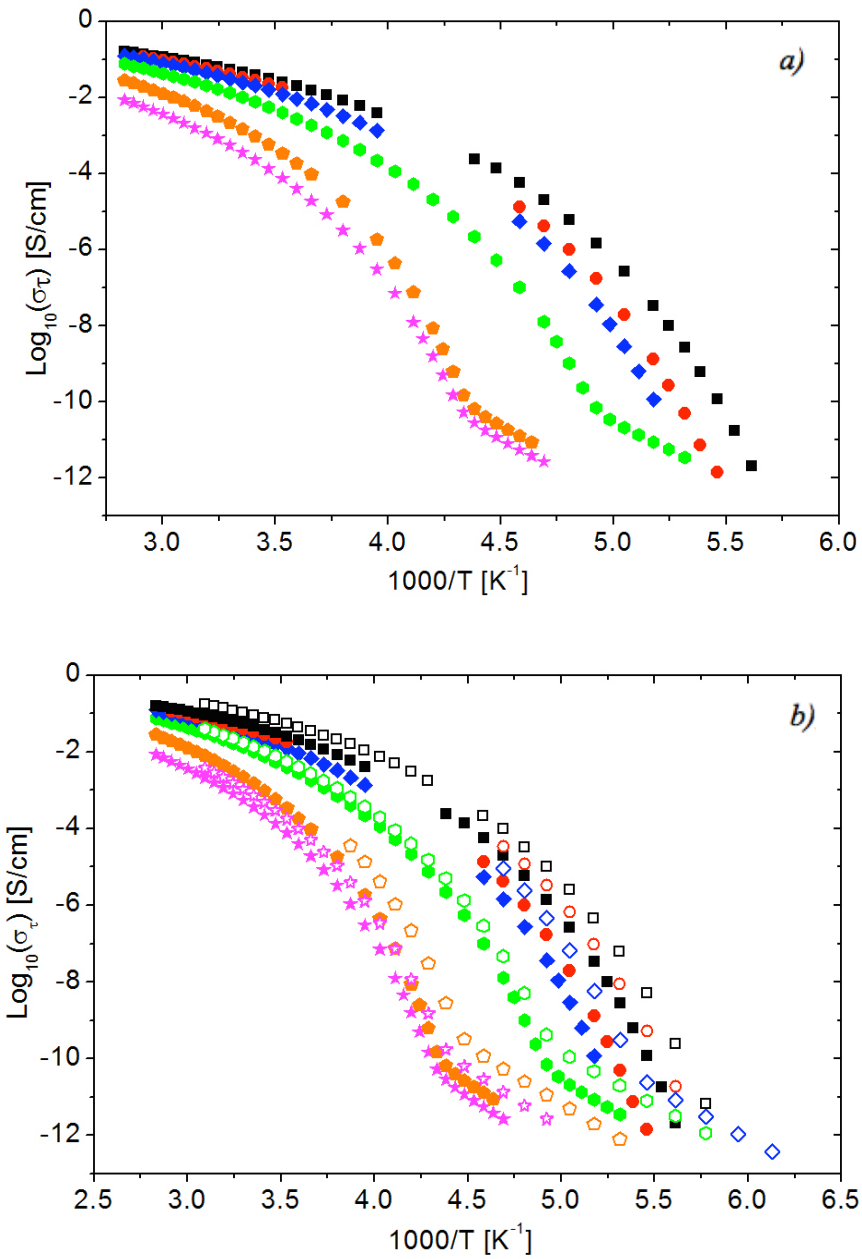

Figure 4.10 Log_{10} of DC conductivity σ_τ of deuterated phosphoric acid at different concentrations a) and the comparison to the hydrated counter parts b) shown in Arrhenius plots. The shown molar ratios correspond to R=1.5 (magenta star), R=2.0 (orange triangle), R=2.5 (green hexagon), R=3.0 (blue diamond), R=4 (red circle) and R=5 (black square) for the deuterated (closed) and hydrogenated (open) samples, respectively.

The difference in σ_τ between isotopes strongly increases with decreasing temperature when approaching the glass transition temperature. Close to T_g the difference extends to nearly one order of magnitude for R=1.5 and more than two orders of magnitude for R=5.

This difference in conductivity between isotopes is even more visible in Figure 4.11, where the ratio of DC conductivity in hydrogenated and deuterated samples is presented. The red dotted line indicates the expected in a simplistic classical model value of $\sqrt{2}$. The ratio of conductivities approaches this limit at higher temperatures, but clearly diverges by orders of magnitude at lower temperatures.

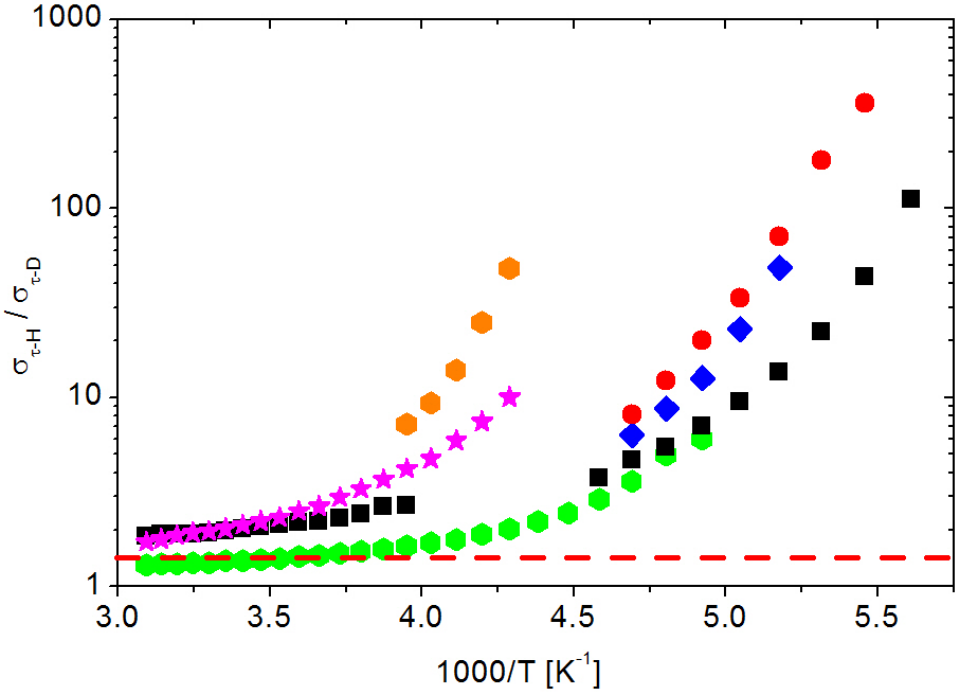

Figure 4.11 Ratio of σ_τ in hydrogenated phosphoric acid to σ_τ in deuterated phosphoric acid vs. 1000/T. The red dotted line indicates a value of $\sqrt{2}$. The molar ratios correspond to R=1.5 (magenta star), R=2.0 (orange triangle), R=2.5 (green hexagon), R=3.0 (blue diamond), R=4 (red circle) and R=5 (black square).

This divergence is caused in part by the shift in Tg between hydrogenated and deuterated samples, as was discussed in previous section. The temperature dependence of σ_τ strongly increases approaching the glass transition. Slight differences in Tg therefore cause a significant difference in conductivity data of the deuterated and hydrogenated samples around T_g. At high temperatures, however, the ratio $\sigma_\tau(H)/\sigma_\tau(D)$ converges to values between one and two for R=1.5, 2.5, 5. High temperature data for sample ratios R=2, 3, 4 were not available for hydrated phosphoric acid samples and are omitted in this analysis.

In order to exclude effects of the glass transition on further data analysis and focus on the high temperature regime, the conductivity data is fit using Vogel-Fulcher-Tammann (VFT), eq. 2.2, and Cohen Grest (CG) eq. 2.3 functions. Both fitting functions were discussed in detail in the chapter 3. Figure 4.12 depicts conductivity data of deuterated phosphoric acids of ratio R=1.5, 2.5, 5, fitted to the VFT (red) and CG (green) functions above T_g. While the VFT function fits the data relatively well and is the common method of analyzing these data [34, 45], the CG function provides a more accurate fit at higher temperatures due to an additional fitting parameter (VFT has 3 free fit parameters, while CG has 4). This allows for a more accurate extrapolation of conductivity to infinite temperature $\sigma_{T=\infty}$ with the CG function.

Since conductivity increases with temperature, $\sigma_{T=\infty}$ resembles the maximum possible conductivity of a material. The ratio of this extrapolated $\sigma_{T=\infty}$ of hydrogenated to deuterated phosphoric acid is depicted in the insert in Figure 4.12. Here the ratios of fitting parameters of VFT and Cohen Grest functions are presented by the red and blue squares, respectively. In addition, the values of the highest temperature data points are compared as well. Although the data is fairly scattered, they are all around value ~1.5 for all the samples. This is close to the expectations of a classical isotope effect.

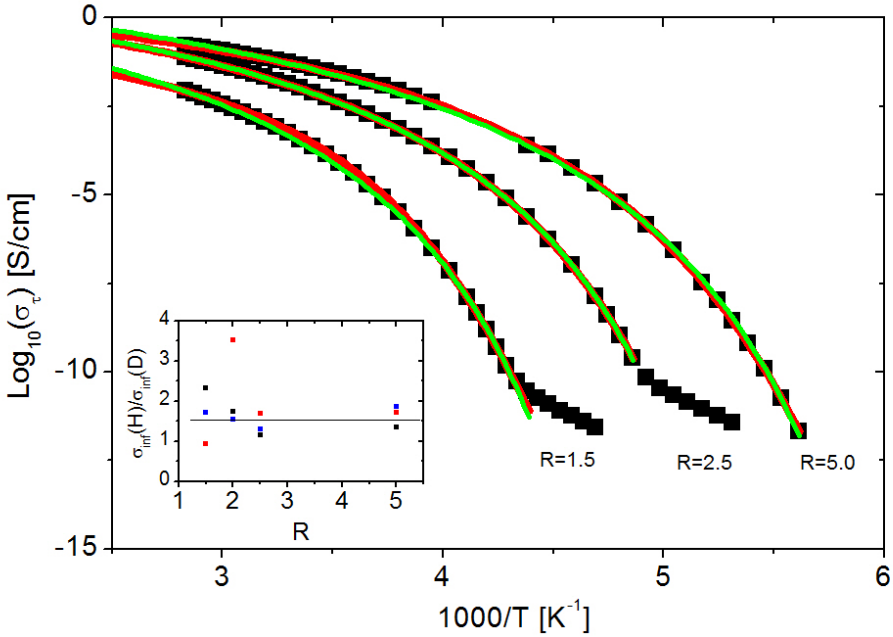

Figure 4.12 shows σ_τ of deuterated phosphoric acid at Ratios R=1.5, 2.5, 5.0 (indicated on plot). The VFT (red) and Cohen Grest (green) fitting functions are extrapolated to $\sigma(T = \infty)$. The insert shows the ratio of the $\sigma(T = \infty)$ in hydrogenated to $\sigma(T = \infty)$ in deuterated phosphoric acids obtained from the VFT fit (red squares) and Cohen Grest fit (black squares). The blue squares denote the same ratio taken from the experimental data at 50℃.

Discussion of Ionic Conductivity

The isotope effect has been previously shown to have strong impact on conductivity behavior of proton conducting materials [46, 47]. Phosphoric acid has been suggested to be a model system of study due to its excellent glass forming and proton conducting properties. Though well studied at high temperatures, the isotope effect on proton conductivity in the low temperature region has not been extensively studied

In the high temperature regime the isotope effect is not as pronounced as it is close to T_g (Figure 4.11). DC conductivity of the phosphoric acid samples prepared with H_2O was between 1 to 2 times higher than that of the samples prepared with D_2O. Though scattered, the data corresponds well to that of the classically predicted ratio of $\frac{\sigma_\tau(H)}{\sigma_\tau(D)} = \sqrt{2}$. These findings are also in agreement with values found in the literature [20, 22, 39]. At high temperatures, molecular motion is not restrained, as it is in the glassy state, and ions can diffuse freely. With decreasing temperature the change in physical properties of the sample have a stronger impact on ion dynamics in the deuterated samples. The decrease in DC conductivity and an increase in conductivity relaxation time are more pronounced in deuterated than in hydrogenated phosphoric acid.

Experimental results on conductivity relaxation time and activation energy indicate that ionic motion does not scale with the square root of the ratio of mass at temperatures close to and below the glass transition. Conductivity relaxation times at the glass transition display a very prominent isotope effect. Deuterated phosphoric acid samples relax a minimum of 3 times slower compared to their hydrogenated counterparts for concentrated samples. The isotope effect increases to over 7 times within the measured concentration range. The difference in glass transition temperatures of the deuterated and hydrogenated samples has to be taken into account during this evaluation. Due to strong temperature dependence of τ_σ directly above the glass transition, small changes in T_g can cause vast differences in relaxation times. The ratio of relaxation times at a fixed temperature may, therefore, not be a fair direct comparison due to the ΔT_g between isotopes discussed in an earlier section. Comparison of τ_σ at Tg is better in that case, because it provides comparison of τ_σ at the same structural relaxation time. τ_σ of the

deuterated sample is always higher across the entire measured range, regardless of change in glass transition temperature.

Below the glass transition temperature, ions can only move via the Grotthuss type hopping mechanism [20]. The classical model of proton transport eq. 2.5 is insufficient in describing the isotope effect in this region. A comparison of the activation energies of ionic conduction below T_g of deuterated and hydrated phosphoric acid also shows a significant Isotope effect. The activation energies of deuterium are 6-7 $\frac{kJ}{mol}$ higher than for proton conduction in phosphoric acids. Additionally the isotope effect increases with increasing water content, with the ratio of activation energies increasing from 1.06 for R=1.5 to 1.13 for R=4.

Semi-classical theories predict that the ion, which is attempting to overcome a certain potential energy barrier, is aided by quantum mechanical ground state energy [21, 46]. The amount of energy that the particle needs to gain in order overcome the potential barrier is reduced by the amount of the ground state energy. This energy originates from zero point vibrations of the proton/ion. Since lighter particles vibrate faster they possess a greater zero point energy than heavier ones, causing the necessary activation energy to decrease in contrast. The result of such a semi-classical effect would further increase isotopic effects in proton conduction. The difference in ionic conductivity between isotopes has also been analyzed theoretically using quantum-tunneling effects. This theory builds on the semi-classical theory and adds a small probability of tunneling under the potential energy barrier. The lighter ion has much greater probability of tunneling, further explaining the isotope effects below the glass transition. Furthermore the increase of the isotope effect in activation energy with decreasing temperature could be explained due to the increased probability of quantum effects at lower temperatures. However no convincing evidence for quantum effects exists in our data.

The general trend in these data is that the isotope effect increases with decreasing acid concentration and decreasing temperature. A greater number of H_2O or D_2O to phosphorus pentoxide molecules creates a larger difference in properties of the sample. By this logic the highest isotope effect can be achieved in the dilute limit of the phosphoric acid where normal water and heavy water dominate the composition of the sample. The dilution of the phosphoric acid drives the interesting properties to lower temperatures, and one could argue that it is not the increasing molar amount of H_2O and D_2O, but rather the decreasing temperatures that drive the increasing isotope effect. Indeed, all quantum effects are expected to be stronger at lower temperatures where normal over-barrier relaxations are strongly suppressed. It is difficult to determine the exact cause of the increase in isotope effect in this case, due to the interconnected nature of decreasing temperature effects with increasing dilution of the sample.

CHAPTER 5:

CONCLUDING REMARKS

The goal of this study was to investigate the isotope effect on glass transition and proton conduction in phosphoric acid. Phosphoric acid has a wide range of applications ranging from biology to industry. Some favorable characteristics include excellent glass forming capability upon vitrification, as well as the highest intrinsic proton conduction amongst common acids. It has been shown that the Grotthuss mechanism is responsible for fast proton conductivity, which leads to the question whether the process follows a purely classical nature, or if quantum effects become apparent. The isotope effect allows for a variation of mass of the conducting ion while charge remains constant. The mass dependence of charge transport characteristics can then shed light onto the classical or quantum nature of the processes.

It was shown using broadband dielectric spectroscopy, differential scanning calorimetry and Brillouin light scattering, that the isotope effect causes an increase in the glass transition temperature and that the difference in T_g between the deuterated and hydrogenated acids increases with molar concentration of H_2O and D_2O.

The isotope effect also causes a decrease in conductivity in the sample containing the heavier isotope and an increase in proton transition time at the glass transition temperature. The ratio of τ_σ of the two isotopes not only far exceeds the classically predicted dependence of $\frac{\tau_\sigma(D)}{\tau_\sigma(H)} \propto \sqrt{2}$, but also further increases with the dilution of the acid. The isotope effect on activation energy of ionic conduction also increase with dilution, which is not predicted by classical theory. These inconsistencies with classical theory could suggest possible influence of quantum effects, but no definite conclusions can be made from these data.

Studies of viscosity measurements for Walden plot analysis which give rise to the degree of decoupling of ionic transport from structural dynamics will be very helpful in future studies. In addition, it would be of interest to measure molecular motion using dynamic light scattering. These measurements can provide further information about molecular dynamics and change of physical properties, which influence proton conduction.

Phosphoric acids are widely used in proton conducting polymer electrolytes and membranes, where decoupling of proton conduction from structural relaxation is a desired attribute. Further understanding of the decoupling phenomena in phosphoric acids and other proton conducting materials can aid the design of novel materials for industry and energy application.

LIST OF REFERENCES

1. Anderson, P.W., *Through the Glass Lightly.* Science, 1995. **267**(5204): p. 1615-1616.
2. Debenedetti, P.G. and F.H. Stillinger, *Supercooled liquids and the glass transition.* Nature, 2001. **410**(6825).
3. Sokolov, A.P., *Why the Glass Transition Is Still Interesting.* Science, 1996. **273**(5282): p. 1675-1676.
4. Kreuer, K.D., Chem. Mater., 1996. **8**: p. 610.
5. Kreuer, K.D., et al., Chem. Rev., 2004. **104**: p. 4637.
6. Kreuer, K.-D., et al., *Transport in Proton Conductors for Fuel-Cell Applications: Simulations, Elementary Reactions, and Phenomenology.* Chemical Reviews, 2004. **104**(10): p. 4637-4678.
7. Tuckerman, M., et al., *Ab Initio Molecular Dynamics Simulation of the Solvation and Transport of H 3 0 + and OH- Ions in Water.* J. Phys. Chem., 1995. **99**: p. 5749.
8. Tuckerman, M.E., D. Marx, and M. Parrinello, Nature, 2002. **417**: p. 925.
9. Tuckerman, M., et al., J. Chem. Phys., 1995. **103**: p. 150.
10. Noam, A., *The Grotthuss Mechanism.* Chemical Physics Letters, 1995. **244**.
11. Marx, D., *Proton Transfer 200 Years after von Grotthuss: Insights from Ab Initio Simulations.* ChemPhysChem, 2006. **7**(9): p. 1848-1870.
12. Vilciauskas, L., et al., *The mechanism of proton conduction in phosphoric acid.* Nat Chem, 2012. **4**(6): p. 461-6.
13. VilÄ iauskas, L., et al., *The mechanism of proton conduction in phosphoric acid.* Nature, 2012. **4**(6).
14. Wojnarowska, Z., et al., *Anomalous Electrical Conductivity Behavior at Elevated Pressure in the Protic Ionic Liquid Procainamide Hydrochloride.* Physical Review Letters, 2012. **108**(1): p. 015701.
15. Trachenko, K., *The Vogel–Fulcher–Tammann law in the elastic theory of glass transition.* Journal of Non-Crystalline Solids, 2008. **354**(32): p. 3903-3906.
16. Cohen, M.H. and G.S. Grest, *Liquid-glass transition, a free-volume approach.* Physical Review B, 1979. **20**(3): p. 1077-1098.
17. Griffin, P.J., et al., *Dynamic crossover and the Debye-Stokes-Einstein relation in liquid N,N-diethyl-3-methylbenzamide (DEET).* Soft Matter, 2013. **9**(43): p. 10373-10380.
18. Mukundan, R., et al., *Tritium Conductivity and Isotope Effect in Proton-Conducting Perovskites.* Journal of The Electrochemical Society, 1999. **146**(6): p. 2184-2187.
19. Kreuer, A. Fuchs, and J. Maier, *H/D isotope effect of proton conductivity and proton conduction mechanism in oxides.* Solid State Ionics, 1995. **77**.
20. Agmon, N., *The Grotthuss mechanism.* Chemical Physics Letters, 1995. **244**(5–6): p. 456-462.
21. Nowick*, A.S. and A.V. Vaysleyb, *Isotope effect and proton hopping in high-temperature protonic.* Solid State Ionics, 1997. **97**: p. 17.
22. Aihara, Y., et al., *Ion Conduction Mechanisms and Thermal Properties of Hydrated and Anhydrous Phosphoric Acids Studied with 1H, 2H, and 31P NMR.* The Journal of Physical Chemistry B, 2006. **110**(49): p. 24999-25006.
23. Johari, G.P., A. Hallbrucker, and E. Mayer, *Isotope effect on the glass transition and crystallization of hyperquenched glassy water.* The Journal of Chemical Physics, 1990. **92**(11): p. 6742-6746.

24. Johari, G.P., A. Hallbrucker, and E. Mayer, *Isotope and impurity effects on the glass transition and crystallization of pressure-amorphized hexagonal and cubic ice.* The Journal of Chemical Physics, 1991. **95**(9): p. 6849-6855.
25. Elsaesser, M.S., et al., *Reversibility and isotope effect of the calorimetric glass. liquid transition of low-density amorphous ice.* Physical Chemistry Chemical Physics, 2010. **12**(3): p. 708-712.
26. C. Gainaru, et al., PNAS, (Submitted).
27. Hitoshi Kanno, I.S., Shegeru Minomura, *Isotope Effect of the Glass Transition Temperature of Aqueous Solution. LiCl and ZnCl2 Solutions in Water and D2O.* The Chemical Society of Japan, 1980. **53**: p. 2079-2080.
28. Lesikar, A.V., *Comment on ''The composition dependence of glass transition properties''.* The Journal of Chemical Physics, 1978. **68**(7): p. 3323-3325.
29. Angell, C.A., J.M. Sare, and E.J. Sare, *Glass transition temperatures for simple molecular liquids and their binary solutions.* The Journal of Physical Chemistry, 1978. **82**(24): p. 2622-2629.
30. Kreuer, K.D. Paddison, S. § Eckhard Spohr,# and Michael Schuster, *Transport in Proton Conductors for Fuel-Cell Applications Simulations Elementary reactions and Phenomenology.* Chemical Reviews, 2004. **104**.
31. Kreuer, K.D., *On the development of proton conducting polymer membranes for hydrogen and methanol fuel cells.* Journal of Membrane Science, 2001. **185**.
32. ELLIS, B., *The glass transition temperatures of phosphoric acids.* Nature, 1976. **263**: p. 674-676.
33. Corti, H.R., F.J. Nores-Pondal, and C.A. Angell, *Heat capacity and glass transition in P2O5-H2O solutions: support for Mishima's conjecture on solvent water at low temperature.* Phys Chem Chem Phys, 2011. **13**(44): p. 19741-8.
34. Wang, Y., et al., *Ionic conductivity and glass transition of phosphoric acids.* J Phys Chem B, 2013. **117**(26): p. 8003-9.
35. Martin, S.W. and C.A. Angell, *On the glass transition and viscosity of phosphorus pentoxide.* The Journal of Physical Chemistry, 1986. **90**(25): p. 6736-6740.
36. Gordon, M. and J.S. Taylor, *Ideal copolymers and the second-order transitions of synthetic rubbers. i. non-crystalline copolymers.* Journal of Applied Chemistry, 1952. **2**(9): p. 493-500.
37. Blander, M., et al., *Solubility of Noble Gases in Molten Fluorides. II. In the Lif–NaF–LF Eutectic Mixtures.* The Journal of Physical Chemistry, 1959. **63**(7): p. 1164-1167.
38. Kreuer, K.-D., *Proton Conductivity: Materials and Applications.* Chemistry of Materials, 1996. **8**(3): p. 610-641.
39. Marx, D., *Proton transfer 200 years after von Grotthuss: insights from ab initio simulations.* Chemphyschem, 2006. **7**(9): p. 1848-70.
40. Franck, E.U., *Electrolyte Solutions, von R. A. Robinson und R. H. Stokes. — The Measurement and Interpretation of Conductance, Chemical Potential and Diffusion in Solutions of Simple Electrolytes. Butterworths Scientific Publication, London 1959. 2. Aufl., XV, 559 S., geb. £ 3.5.0.* Angewandte Chemie, 1960. **72**(12): p. 426-426.
41. Kremer and Schönhals, *Broadband Dielectric Spectroscopy*. 2002, New York: Springer.
42. Hong, L., *MOLECULAR COOPERATIVITY IN THE DYNAMICS OF GLASS-FORMING MATERIALS*. 2010, The University of Akron.

43. Bockris, J.O.M. and A.K.N. Reddy, *Modern Electrochemistry*. 1970, New York: Plenum Press. 470-486.
44. Bernal, J.D. and R.H. Fowler, *A Theory of Water and Ionic Solution, with Particular Reference to Hydrogen and Hydroxyl Ions.* The Journal of Chemical Physics, 1933. **1**(8): p. 515-548.
45. Griffin, P., et al., *Decoupling charge transport from the structural dynamics in room temperature ionic liquids.* The Journal of Chemical Physics, 2011. **135**(11): p. -.
46. Kreuer, K.D., T. Dippel, and J. Maier, *H/D isotope effect of proton conductivity and proton conduction mechanism in oxides.* Proc. Electrochem. Soc., 1995: p. 95.
47. Slade, R.C.T. and N. Singh, *Generation of charge carriers and an H/D isotope effect in proton-conducting doped barium cerate ceramics.* Journal of Materials Chemistry, 1991. **1**(3): p. 441-445.

VITA

Max was born in Austin, TX in 1989, but grew up in Germany near the city Bonn. After the completion of his 10th year of Gymnasium (Germany's highest form of high school), Max moved to America to begin a foreign exchange year in the United States in 2005. Max decided to stay in the US to complete his high school career. In 2007, he began his undergraduate studies at Dalton State College followed by a transferred to the University of West Georgia in fall of 2009. Max received his degree of Bachelors of Science in Physics in May of 2011. Max got accepted to the University of Tennessee Knoxville (UTK) Physics department, where he joined the group of Dr. Alexei Sokolov at the beginning of summer of 2011. After three years of classwork and research at UTK and Oakridge National Laboratories, Max will receive his masters degree in Physics in August 2014, and move on to further graduate work in the Chemical and Bio-molecular Engineering department at UTK starting in the fall of 2014.